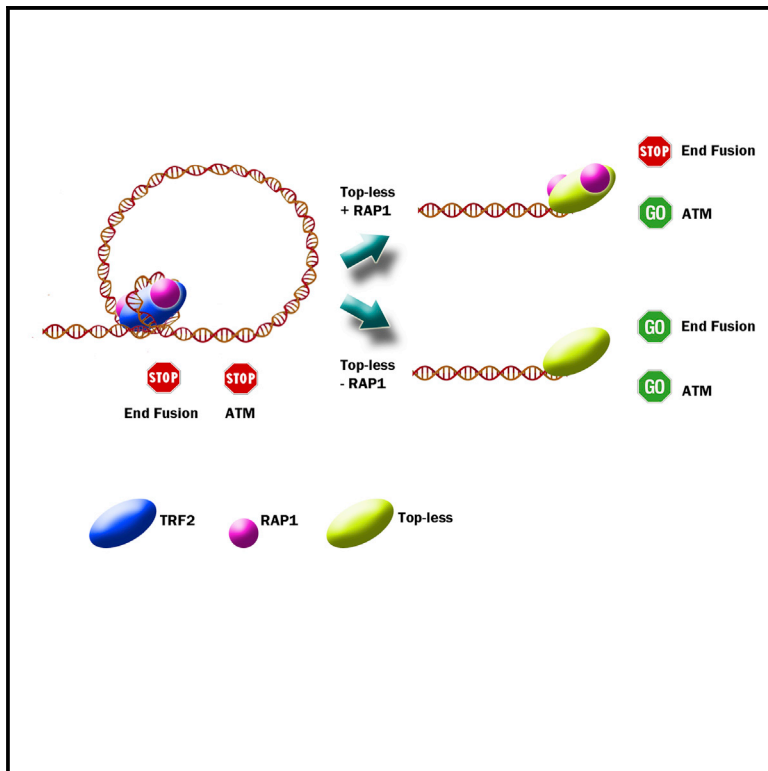


TRF2-Mediated Control of Telomere DNA Topology as a Mechanism for Chromosome-End Protection

Graphical Abstract



Authors

Delphine Benarroch-Popivker,
Sabrina Pisano,
Aaron Mendez-Bermudez, ...,
Hong Wang, Eric Gilson,
Marie-Josèphe Giraud-Panis

Correspondence

eric.gilson@unice.fr (E.G.),
giraud-panis@unice.fr (M.-J.G.-P.)

In Brief

Benarroch-Popivker et al. show that TRF2 wraps DNA around its TRFH domain, thereby controlling telomeric DNA topology, t-loop formation, and ATM inhibition. In TRF2 wrapping-deficient cells, protection of telomeres against fusion relies on the recruitment of RAP1.

Highlights

- TRF2 modifies DNA topology by wrapping 90 base pairs of DNA around its TRFH domain
- A mutant deficient in DNA wrapping, Top-less, causes relaxation of telomeric DNA
- Top-less telomeres are deprotected and harbor fewer t-loops but are not fused by NHEJ
- RAP1 protects Top-less telomeres against fusions



TRF2-Mediated Control of Telomere DNA Topology as a Mechanism for Chromosome-End Protection

Delphine Benarroch-Popivker,^{1,9} Sabrina Pisano,^{1,9} Aaron Mendez-Bermudez,^{1,2} Liudmyla Lototska,¹ Parminder Kaur,³ Serge Bauwens,¹ Nadir Djerbi,¹ Chrysa M. Lattrick,^{1,12} Vincent Fraissier,⁴ Bei Pei,¹ Alexandre Gay,^{1,11} Emilie Jaune,¹ Kevin Foucher,¹ Julien Cherfils-Vicini,¹ Eric Aeby,^{5,14,15} Simona Miron,^{6,13} Arturo Londoño-Vallejo,⁷ Jing Ye,² Marie-Hélène Le Du,⁶ Hong Wang,³ Eric Gilson,^{1,2,8,10,*} and Marie-Josèphe Giraud-Panis^{1,10,*}

¹Institute for Research on Cancer and Aging, Nice (IRCAN), Faculty of Medicine, CNRS UMR7284, INSERM U1081, University of Nice Sophia Antipolis, Nice, France

²International Laboratory in Hematology and Cancer, Shanghai Jiao Tong University School of Medicine/Ruijin Hospital/CNRS/INSERM/Nice University, Pôle Sino-Français de Recherche en Sciences du Vivant et Génomique, Shanghai Ruijin Hospital, Huangpu, Shanghai 200025, P.R. China

³Physics Department, North Carolina State University at Raleigh, Raleigh, NC 27695, USA

⁴Cell and Tissue Imaging Platform (PICT-IBiSA), Nikon Imaging Centre, UMR 144 CNRS Institut Curie, 75248 Paris Cedex 05, France

⁵Swiss Institute for Experimental Cancer Research (ISREC), School of Life Sciences, Ecole Polytechnique Fédérale de Lausanne (EPFL), 1015 Lausanne, Switzerland

⁶Institute for Integrative Biology of the Cell (I2BC), CEA, CNRS, Université Paris-Sud, Bâtiment 144, CEA Saclay, Gif-sur-Yvette F-91191, France

⁷UMR3244, Telomeres and Cancer Laboratory, Institut Curie, Paris 75248, France

⁸Department of Genetics, CHU Nice, Nice 06202, France

⁹Co-first author

¹⁰Co-senior author

¹¹Present address: INSERM UMR944, CNRS UMR7212, University of Paris Diderot, Sorbonne Paris Cité, Hôpital St. Louis, 1 Avenue Claude Vellefaux, 75475 Paris Cedex 10, France

¹²Present address: Département de Génomique Fonctionnelle et Cancer, Institut de Génétique et Biologie Moléculaire et Cellulaire (IGBMC), Université de Strasbourg, CNRS, INSERM, 1 rue Laurent Fries, B.P.10142, 67404 Illkirch Cedex, France

¹³Present address: Institute of Biochemistry, Splaiul Independentei 296, 060031 Bucharest 17, Romania

¹⁴Present Address: Department of Molecular Biology, Massachusetts General Hospital, Boston, MA 02114, USA

¹⁵Present address: Department of Genetics, Harvard Medical School, Boston, MA 02115 USA

*Correspondence: eric.gilson@unice.fr (E.G.), giraud-panis@unice.fr (M.-J.G.-P.)

<http://dx.doi.org/10.1016/j.molcel.2015.12.009>

SUMMARY

The shelterin proteins protect telomeres against activation of the DNA damage checkpoints and recombinational repair. We show here that a dimer of the shelterin subunit TRF2 wraps ~90 bp of DNA through several lysine and arginine residues localized around its homodimerization domain. The expression of a wrapping-deficient TRF2 mutant, named Top-less, alters telomeric DNA topology, decreases the number of terminal loops (t-loops), and triggers the ATM checkpoint, while still protecting telomeres against non-homologous end joining (NHEJ). In Top-less cells, the protection against NHEJ is alleviated if the expression of the TRF2-interacting protein RAP1 is reduced. We conclude that a distinctive topological state of telomeric DNA, controlled by the TRF2-dependent DNA wrapping and linked to t-loop formation, inhibits both ATM activation and NHEJ. The presence of RAP1 at telomeres appears as a backup mechanism to prevent NHEJ when topology-mediated telomere protection is impaired.

INTRODUCTION

Telomeres have evolved in eukaryotes from the need to protect chromosome ends and provide genome stability. Their maintenance requires protection against the DNA damage response (DDR) that would otherwise stop cell division by checkpoint activation and lead to end-to-end fusion by non-homologous end joining (NHEJ). In humans, telomeres consist of a repetitive DNA ending with a single-stranded 3' overhang and organized in a peculiar chromatin structure involving the shelterin protein complex and the noncoding RNA TERRA (Giraud-Panis et al., 2013). Their main function is to protect chromosome ends against DNA damage checkpoints and recombinational repair as well as to assist terminal DNA replication and processing (de Lange, 2005; Gilson and Géli, 2007).

TRF2, one of the shelterin subunits, inhibits NHEJ and the ataxia telangiectasia mutated (ATM)-dependent DDR pathway (Celli and de Lange, 2005; Denchi and de Lange, 2007; Okamoto et al., 2013; van Steensel et al., 1998). TRF2 also protects telomeric sequences against replicative DNA damage, particularly those due to topological stress (Muraki et al., 2011; Saint-Léger et al., 2014; Ye et al., 2010). In order to achieve these functions, TRF2 exhibits numerous activities (Feuerhahn et al., 2015). At its N terminus, a basic domain (B domain) interacts with branched

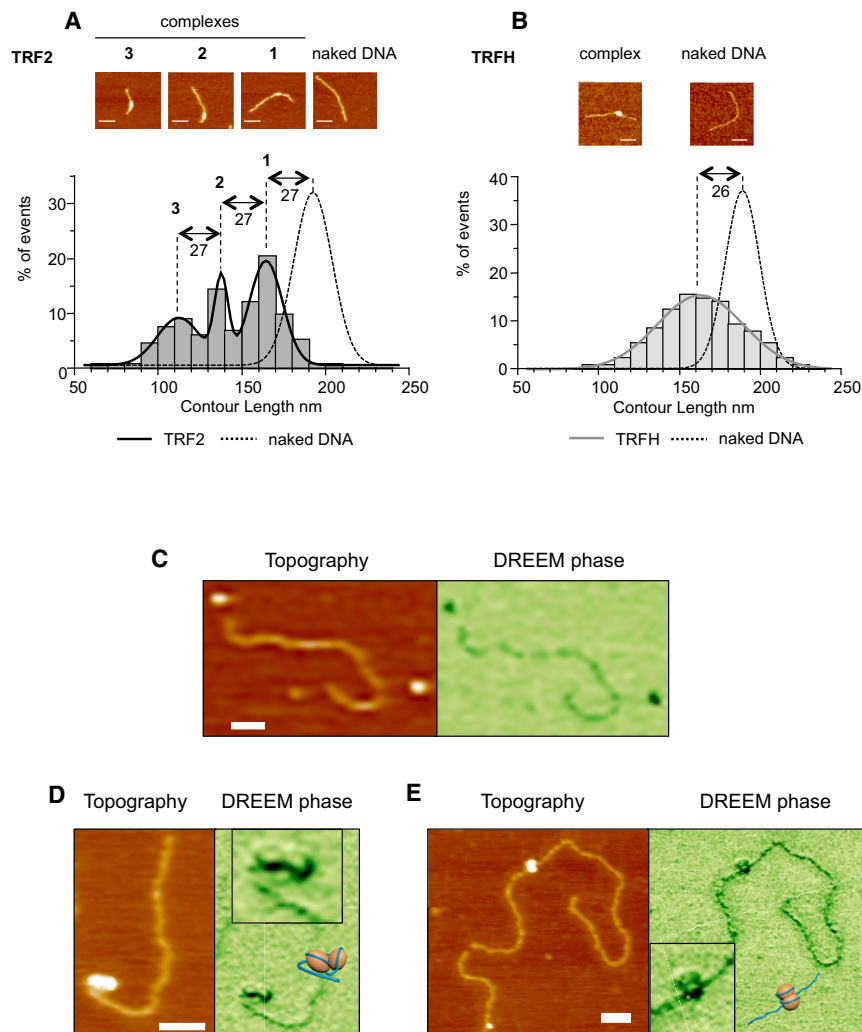


Figure 1. TRFH Domain of TRF2 Condenses ~90 bp of DNA

(A) AFM experiments show a decrease in the contour length (CL) of a 650 bp telomeric DNA fragment due to TRF2 binding. (Top) Representative AFM images; scale bars, 50 nm; (bottom) graph representing CL distribution for free and bound DNA ($n = 133$ for TRF2, $n = 304$ for DNA). Histograms correspond to raw data and curves to the sum of a Gaussian multipole fitting.

(B) Same experiment as in (A) using the TRFH domain ($n = 130$ for TRFH, $n = 154$ for DNA).

(C) Topographic AFM (left panel) and DREEM phase (right panel) images of free TRFH protein molecules and DNA.

(D and E) Representative topographic AFM (left panels) and DREEM phase (right panels) images of TRFH-DNA complexes with telomeric sequences (D, 135 TTAGGG repeats) or a nontelomeric fragment (E, 3.8 kb).

The XY scale bars, 50 nm. Boxed regions in (D) and (E) are zoomed DREEM images from main figures. The TRFH-DNA models are as follows: orange spheres for TRFH dimers and dark blue lines for DNA.

et al., 2009, 2011; Poulet et al., 2012; Verdun and Karlseder, 2006).

In this report, we show that ~90 base pairs (bp) of DNA is wrapped around a TRFH homodimer. This wrapping involves lysines and arginines located on a DNA path, whose mutation compromises TRF2 capacity to induce DNA wrapping in vitro. In human cells, expression of this mutant, named Top-less, causes changes in telomeric DNA topology, a decrease in the amount of t-loops, and defects in telomere protection against DDR. However, chromosome ends are still protected against NHEJ. A reduced expression of RAP1 alleviates this protection. These findings reveal that a distinctive topological state of telomeric DNA, controlled by TRF2-mediated DNA wrapping and linked to t-loop formation, inhibits both ATM activation and NHEJ. The presence of RAP1 at telomeres appears as a backup mechanism to prevent NHEJ when topological-mediated telomere protection is impaired.

However, chromosome ends are still protected against NHEJ. A reduced expression of RAP1 alleviates this protection. These findings reveal that a distinctive topological state of telomeric DNA, controlled by TRF2-mediated DNA wrapping and linked to t-loop formation, inhibits both ATM activation and NHEJ. The presence of RAP1 at telomeres appears as a backup mechanism to prevent NHEJ when topological-mediated telomere protection is impaired.

RESULTS

TRF2 Condenses ~90 bp of DNA through the TRFH Domain

TRF2-mediated DNA condensation can be observed by measuring the length of DNA molecules (DNA contour length, CL) in TRF2-DNA complexes using atomic force microscopy (AFM). As seen in Figure 1A, TRF2 causes a large decrease in CL. Fitting the CL distribution with a multi-Gaussian curve reveals the presence of three types of complexes (CLs of 165 ± 10 , 138 ± 4 , and 111 ± 13 nm). Notably, these CL values and that of the naked DNA (192 ± 11 nm) all differ by multiples of

DNA structures and protects them against resolution (Fouché et al., 2006; Poulet et al., 2009). The homodimerization domain that forms a horseshoe structure in its dimeric form (TRFH for TRF homology domain) (Chen et al., 2008; Fairall et al., 2001) has been shown to suppress ATM activation (Okamoto et al., 2013) and to control TERRA transcription (Porro et al., 2014a, 2014b). This domain also acts as a binding hub for various repair proteins, such as Apollo, SLX4, or RTEL1 (Chen et al., 2008; Kim et al., 2009; Sarek et al., 2015; Wan et al., 2013; Wilson et al., 2013). The hinge domain harbors sites for other protein interactions such as the shelterin subunits RAP1 and TIN2 and also inhibits ATM signaling (Okamoto et al., 2013). Finally, at the C terminus a Myb/SANT domain (Telobox) is responsible for sequence-specific telomeric DNA binding (Bilaud et al., 1996, 1997; Court et al., 2005). TRF2 is also capable of folding telomeric DNA into a lasso-like structure called the t-loop (Griffith et al., 1999; Stansel et al., 2001). This higher-order telomeric DNA structure is believed to play a key role in telomere protection (Doksani et al., 2013) and has been proposed to be linked to the ability of TRF2 to stimulate invasion of duplex telomeric DNA by a homologous single strand (Amiard et al., 2007; Baker

27 nm. Deconvoluted volumes of TRF2-DNA complexes (Figure S1A, available online) also showed a three-peaks distribution. Since the sum of the volumes of one TRFH dimer and two Telobox domains corresponds to 66 nm^3 , the mean deconvoluted volume of complexes in peak 1 ($90 \pm 34 \text{ nm}^3$) is compatible with that of a dimer of the protein (Figure S1A). By inference, the two other types of complexes should correspond to two and three dimers bound to DNA. These analyses revealed that TRF2 dimers can form complexes with DNA, each condensing DNA by $\sim 27 \text{ nm}$ ($\sim 90 \text{ bp}$).

Since TRF2 ability to condense DNA depends on the TRFH domain (Amiard et al., 2007; Poulet et al., 2012), we explored whether this domain is sufficient. Purified TRFH binds DNA, albeit with low affinity (Figures S1B and S1C), and leads to a DNA condensation similar to that of full-length TRF2 (Figure 1B). In agreement, the preferred length of DNA bound by this domain is $\sim 92 \text{ bp}$ (Figures S1D and S1E). We also obtained a multipeak distribution for the deconvoluted volumes compatible with dimers and multimers (Figure S1F). As for the full-length protein, larger TRFH-DNA complexes show smaller contour lengths, and vice versa (Figure S1G). Hence, the Gaussian aspect of the TRFH CL distribution (Figure 1B) is probably a consequence of variations in condensation for the different TRFH complexes, likely due to the weak affinity of TRFH for DNA. Alternatively, other domains such as the N-terminal B domain or the C-terminal Myb/SANT domain of TRF2 may stabilize the wrapped structure and be accessory to this TRFH-driven reaction.

We found a good correspondence between circumference and DNA shortening of TRF2-DNA complexes (Figure S1H). Furthermore, the value of nearly 1 in the slope of the linear fit curve suggests that circumference and DNA shortening increase at the same rate. Thus, dimensions of TRF2-DNA complexes can be described by multiples of $\sim 27 \text{ nm}$ that correspond to both the length of condensed DNA and the circumference of the complexes.

This number is similar to the circumference of $\sim 25 \text{ nm}$ calculated from the 3D structure of the TRFH domain (PDB 1H6O and 3BUA) (Chen et al., 2008; Fairall et al., 2001). This suggested that the circumference of the TRFH/DNA complexes should be similar to that of the full-length protein, and, indeed, we obtained $26 \pm 9 \text{ nm}$ for the smallest TRFH/DNA complex and multiples of $\sim 27 \text{ nm}$ for multimeric complexes (Figure S1I).

Overall, these results strongly suggest that the TRFH domain is encircled by $\sim 90 \text{ bp}$ of DNA. In order to confirm this wrapping, we used a recently developed AFM imaging technique called dual resonance frequency enhanced electrostatic force microscopy (DREEM). In recent studies, DREEM was successfully used to observe DNA wrapping around histone proteins in chromatin, DNA passing through the hMutS α repair protein, and higher-order DNA looping at the edge of multiprotein full-length TRF2-DNA complexes (K.P., D. Wu, J. Lin, P. Countryman, R. Riehn, P.L. Opresko, and H. Wang, unpublished data; Wu et al., 2016). We chose to analyze TRFH-DNA complexes rather than those formed with the full-length protein since the other domains of TRF2 may impede the visualization of the wrapping around TRFH. In DREEM imaging, both free proteins and DNA show a decrease in phase, but proteins show a greater contrast than DNA, thus allowing distinction of both molecules in a com-

plex (Figure 1C). TRFH-telomeric DNA complexes in DREEM phase images show dark regions consistent with protein, and regions with decreased signal consistent with DNA (Figure 1D). The regions with decreased intensities show DNA paths on the TRFH consistent with the wrapping of DNA around this domain. We could also observe wrapping when using a nontelomeric linear DNA fragment (Figure 1E), showing that the DNA wrapping around TRFH is not telomeric DNA-sequence specific.

TRFH Contacts DNA through a Set of Lysine Residues

To identify the TRFH residues in contact with DNA, we performed protein footprinting using *in vitro* acetylation by sulfosuccinimidyl acetate (Figure S2A). This compound specifically acetylates lysines exposed to the solvent, which can be mapped using mass spectrometry (Mendoza and Vachet, 2009). We used lysine acetylation profiles to calculate probabilities of their acetylation (Figure S2B; Experimental Procedures). Physical contact of the protein with another molecule modifies lysine acetylation. Comparing acetylation profiles for unbound and bound TRF2 on a 650 bp of telomeric DNA, we determined the percentage of DNA-dependent protection for each acetylatable lysine (Figure 2A). Lysines not present in the unbound protein profile due to lack of acetylation or partial coverage in mass spectrometry were not analyzed (K140, K495, and K180). TRF2 contains 44 lysines distributed along the sequence, with the exception of the N-terminal basic domain. Binding of the DNA causes variations in acetylation to different degrees. Lysines closer to the DNA in the Telobox structure (Court et al., 2005) are more protected from acetylation, validating this approach (Figure S2C). The acetylation of some lysines in the hinge domain is also modulated upon DNA binding, perhaps due to conformational changes in this domain or to DNA binding. Importantly, marked changes in acetylation were observed in three regions of the TRFH centered on K158, K176, and K242. When positioned on the 3D structure, these lysines could be aligned along a DNA path encircling this domain (Figure 2B). Interestingly, K173, K176, and K179 are located in front for one monomer and in the back for the other monomer, thus introducing chirality in the path around the dimer and forcing DNA strands to cross (Figure S2D).

TRF2 Wraps DNA around Its TRFH Domain

To go further, we constructed a set of TRF2 mutants containing lysine-to-alanine replacement. We focused on the lysines exhibiting highest signals in footprinting (K158, K176, and K242) and their surrounding lysines. Mutants with different numbers of mutated lysines were constructed (Figures S3A and S3B): K241, K242, and K245 in mutant 3K; K158, K173, K176, and K179 in mutant 4K; and all seven of them in mutant 7K. We analyzed the capacity of these mutants to bind and wrap DNA by EMSA and by monitoring their topological activity on a plasmid using the Topoisomerase I relaxation assay (Amiard et al., 2007; Poulet et al., 2012; Figures S3C and 3A; numbers below gels). All mutants were active to different degrees. We concluded that, if these lysines contributed to wrapping, other residues must be involved.

The TRF1 TRFH is also capable of condensing DNA, but in TRF1, this capacity is inhibited by the presence of an acidic N-terminal domain. This suggests that the residues involved in

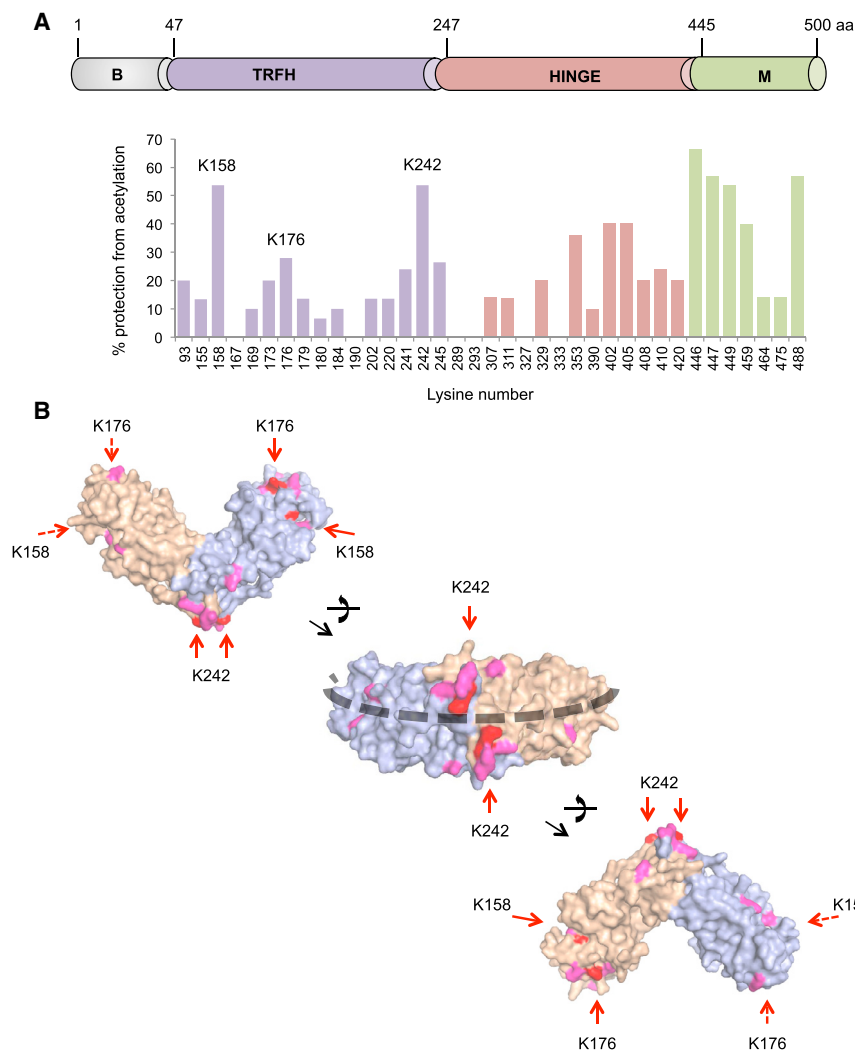


Figure 2. Lysines Involved in DNA Binding Define a “DNA Path” around the TRFH Domain

(A) (Top) Schematic view of TRF2 domains. (Bottom) Footprinting graph showing the percentage of DNA-dependent protection from acetylation for acetylatable lysines (Figure S2).

(B) Positions of protected lysines on the 3D structure of the TRFH domain (PDB: 3BUA). Lysines in red show protection above 20%, and those in pink show protection between 10% and 20%. Lysines on the back of the structures are indicated by dashed arrows. The black dashed line marks the identified DNA path.

DNA wrapping might be conserved between TRF1 and TRF2. Indeed, lysines giving a strong signal in the footprinting assay are either conserved, replaced by an arginine, or only slightly shifted (Figure S3D). Two conserved arginines are located on the putative DNA path (R69 and R99 for TRF2; R91 and R121 in TRF1), and their symmetrical location strongly resembles that of the conserved lysines K245. We mutated these two arginines to alanines in combination with the seven lysines, giving the 7K2R mutant (Figure S3A). This mutant showed reduced topological activity (Figure 3A) and wrapping efficiency (Figure 3B). Similarly, the capacity of 7K2R to stimulate single-strand invasion into a telomeric double helix was strongly impaired (Figures 3C and 3D). These reduced activities did not originate from changes in affinities for telomeric DNA (Figures 3E and 3F) and were not due to the sole mutations of the two arginines since the 2K2R mutant (mutations of K158, K242, and the two arginines) was topologically active (Figure S3E). Overall, we conclude that a set of lysine and arginine residues located on the outer surface of the TRFH domain is required to wrap DNA around it and to confer the topological properties of TRF2. Thus, the 7K2R mutant was dubbed Top-less.

In order to characterize Top-less, we compared its biochemical properties to those of the wild-type protein (Figures S3F–S3K). Circular dichroism experiments showed that mutations in Top-less did not modify the overall folding of the protein (Figure S3G). We also showed that Top-less could bind RAP1 in vitro (Figure S3H). As expected, Top-less mutations caused a marked decrease in the affinity of the TRFH for DNA (Figures S3I and S3J). The capacity of TRF2 to promote formation of Holliday junctions and to inhibit their migration, a property a priori unrelated to DNA topology, was unaffected (Figure S3K). We also explored whether Top-less could bind telomeric DNA in vivo. For this purpose, we used a HeLa cell line where TRF2 expression could be severely decreased by expression of a doxycycline (DOX)-inducible shRNA directed against *TERF2* (Grolimund et al., 2013). Cells treated with DOX were transduced with lentiviral vectors expressing either wild-type or Top-less Myc-tagged forms of TRF2 (resistant to the inducible shRNA). Ectopic expression of both wild-type TRF2 and Top-less restored a level of protein that exceeded the endogenous amount observed in cells not treated with DOX (Figure S4A). Binding to telomeres was examined using chromatin immunoprecipitation (ChIP) using either an anti-TRF2 or an anti-Myc antibody (Figures S4B and S4C, respectively). No obvious difference was observed between wild-type and Top-less. Finally, we checked that Top-less modified neither the expression of the other shelterin subunits nor the association of RAP1 and TIN2 at telomeres (Figures S4D–S4G).

Overall, these data show that Top-less is a valuable separation-of-function mutant of TRF2 and is deficient for DNA wrapping activity, but it still exhibits several of the known properties of this protein.

TRF2 Controls Telomeric DNA Topology in Human Cells

Next, we investigated whether DNA wrapping plays a role in the control of telomere DNA topology in human cells. To monitor

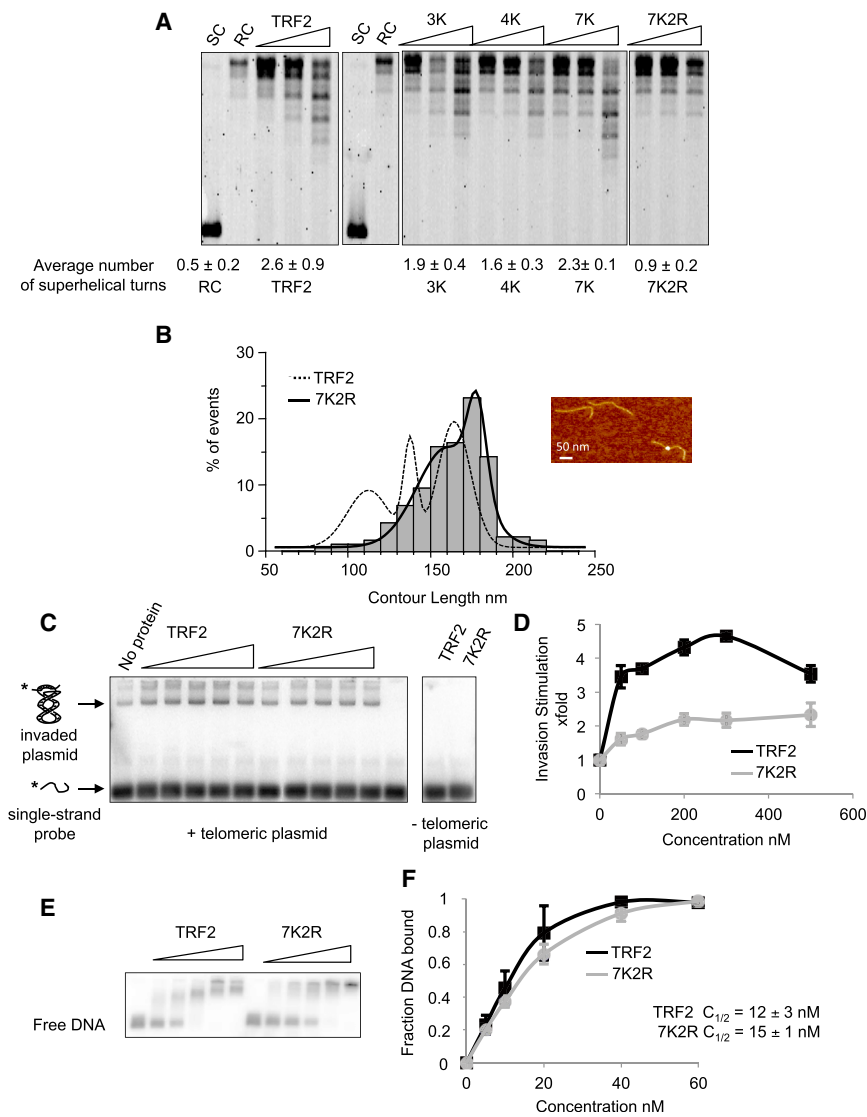


Figure 3. Biochemical Characterization of a Topology-Deficient TRF2 Mutant

(A) Topoisomerase I assay showing the topological activity of TRF2 and of lysine/arginine to alanine mutants. Protein concentrations used were 100, 250, and 500 nM. Average number of helical turns was calculated at 500 nM for at least 3 experiments. SC stands for supercoiled, and RC stands for relaxed circular.

(B) AFM experiments showing the decreased wrapping activity of 7K2R. The graph represents CL distribution for the TRF2- and 7K2R-bound DNA ($n = 133$ for TRF2, $n = 190$ for 7K2R). Histograms correspond to raw data and curves to the sum of Gaussian curves fitting the raw data.

(C) Invasion assay showing the decrease in invasion caused by 7K2R mutations. Concentrations used were 50, 100, 200, 300, and 500 nM for both proteins.

(D) Quantitative analysis of (C). Error bars correspond to standard deviation from three experiments.

(E) EMSA using ds106Telo and either TRF2 or 7K2R. Concentrations used were 5, 10, 20, 40, and 60 nM of proteins.

(F) Quantitative analysis of (E). Error bars represent SD from three experiments.

changes in the DNA topological state, we used the capacity of Trioxsalen (4,5',8-trimethylpsoralen) to bind preferentially to unwound genomic regions and to crosslink DNA strands when exposed to UV. To validate this approach, we performed experiments on cells treated with ICRF-193, a catalytic inhibitor of Topoisomerases 2 (Chen et al., 2015; d'Alcontres et al., 2014; Hsieh et al., 2015; Ye et al., 2010). HeLa cells were incubated with Trioxsalen for 5 min and immediately exposed to UV before recovery of the cells. Hence, the binding profile of Trioxsalen provides a snapshot of the topological state of DNA. As controls, cells were treated with Trioxsalen but not exposed to UV, or vice versa. Trioxsalen DNA crosslinking was quantified on sonicated genomic DNA after denaturation of DNA fragments by glyoxal and separation of crosslinked species (double stranded) and noncrosslinked species (single stranded) by electrophoresis (Kouzine et al., 2013). We verified that fragments were of equivalent length (between 210 and 230 bp) using a Bioanalyzer (an example is given in Figure S5A). After migration, gels were

stained with SYBR green II following a denaturing step to remove Trioxsalen. The SYBR green II image obtained thus reflected genome-wide binding of Trioxsalen. To quantify the crosslinked (double stranded) material, we used a 0.6 kb threshold because it corresponded to an inflection point in the telomeric DNA profiles (Figure S5B). We analyzed telomeric DNA by hybridization of the membrane obtained by Southern blot of the SYBR gel with a telomeric probe (Figure S5D). Under our conditions, ~20% of genomic DNA was crosslinked (~1 Trioxsalen

every kilobase). Interestingly, ICRF-193 treatment causes a detectable increase in Trioxsalen crosslinking of telomeric DNA but not of bulk DNA, indicative of a telomere-specific effect on DNA topology (Figure S5E). It may appear counterintuitive to observe an increase in Trioxsalen binding when inhibiting an enzyme that removes DNA-positive supercoils, but this could be due to topology-driven regression of replication forks (Yeeles et al., 2013) or replication/transcription forks stalling, resulting in the accumulation of unwound regions.

Next, HeLa cells were treated with DOX and transduced with either the empty, TRF2, or Top-less lentiviral vectors as above. The binding of Trioxsalen to global genomic DNA does not depend on TRF2 (Figures 4A and 4C), as expected. However, a nearly 2-fold increase in crosslinked telomeric species is observed when treating HeLa cells with DOX. This topological change is rescued by the expression of wild-type TRF2. In contrast, the expression of Top-less fails to rescue topological changes triggered by TRF2 downregulation (Figures 4B and 4C).

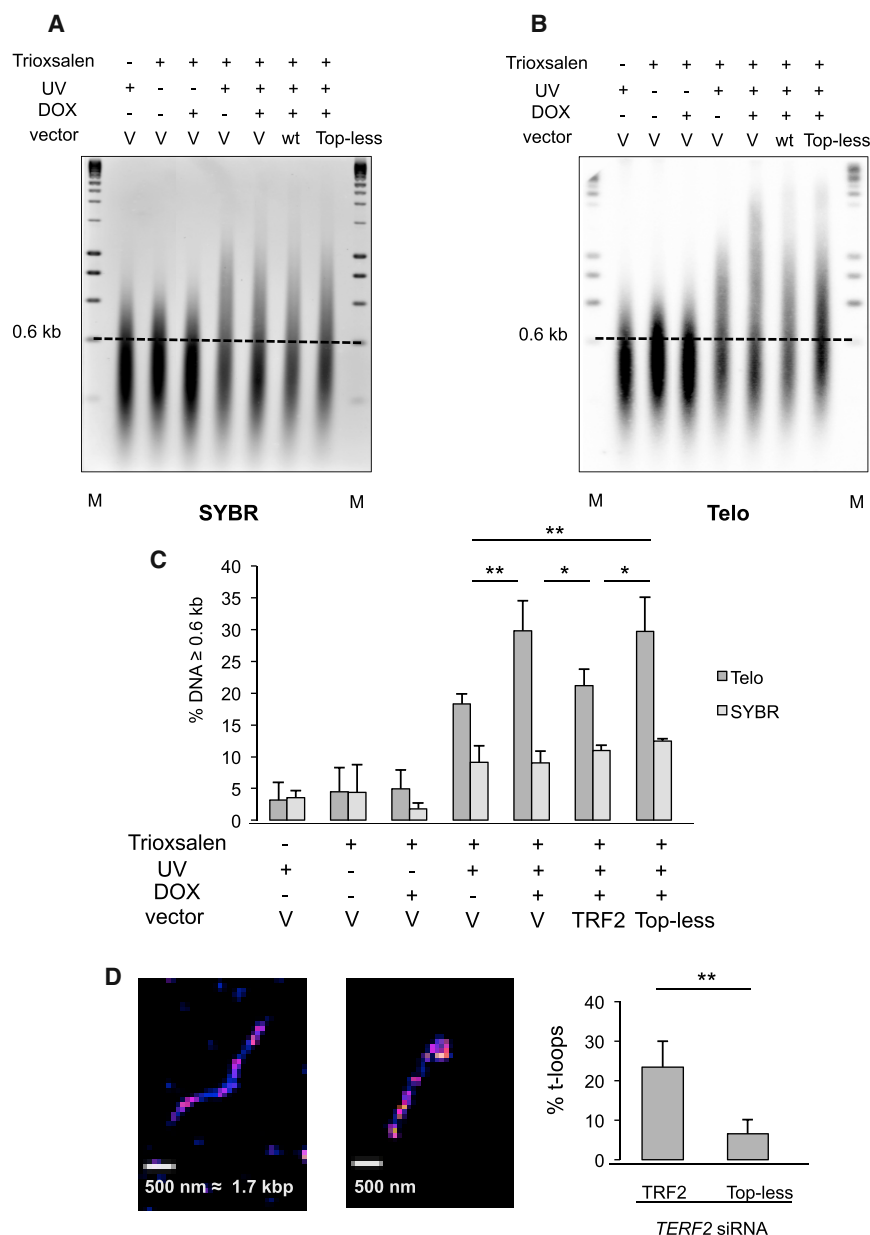


Figure 4. The TRFH-Wrapping Domain of TRF2 Controls Telomeric DNA Topology and t-Loops

(A) SYBR-stained glyoxal gel. M stands for molecular weight markers, V stands for empty vector, wt stands for wild type TRF2, and the dotted line marks the 0.6 kb threshold used for analysis. Of note, a nonrelevant lane was removed from the image, and glyoxal in the samples slows migration compared to the markers.

(B) Southern blot of the glyoxal gel hybridized using a telomeric probe (Telo). As above, a nonrelevant lane was removed from the image.

(C) Quantitative analysis of (B). The relative amount of DNA material above the 0.6 kb mark was measured for each condition. SYBR indicates the values obtained for the SYBR-stained gels, and Telo for the Southern blots. Error bars correspond to standard errors between three replicates. p values were calculated using the Mann-Whitney test (**p < 0.01, *p < 0.05; absence of mark indicates no significance).

(D) Representative images of linear (left) DNA and t-loop (right) obtained on spread chromatin of HT1080 super Telomerase cells by STORM and quantification of the percentage of t-loops in TRF2- (437 objects counted) or Top-less (634 objects counted)-expressing cells. Quantification of *TERF2* transcripts was performed by RT-qPCR and corresponded to a 77% knockdown of the endogenous *TERF2* transcript, while in TRF2 and Top-less conditions the ectopic mRNA was 9.5-fold and 6.5-fold more expressed, respectively, than in the endogenous *TERF2* mRNA in the si-Control condition. Data represent the means \pm SE. p values were calculated using the Mann-Whitney test (**p < 0.01).

These results demonstrate a functional link between the intrinsic ability of TRF2 to wrap DNA and the in vivo control of telomere DNA topology.

TRF2-Mediated DNA Wrapping Controls t-Loops

Two facts suggested that Top-less could lead to variations in the t-loop

content in cells: (1) the reduced capacity of this mutant to stimulate single-strand invasion in vitro (Figure 3C), a property thought to be involved in t-loop formation; (2) the telomere topological change caused by this mutant that could be linked to a loss of constraining structures such as t-loops. In order to investigate this, we performed direct stochastic optical reconstruction microscopy (STORM) imaging as described by Doksani et al. (2013). In order to increase our chances to observe t-loops, we used HT1080 cells overexpressing telomerase which can harbor telomeres of more than 20 kb (Cristofari and Lingner, 2006). Endogenous TRF2 expression was reduced by transfection of a siRNA directed against TRF2, and wild-type TRF2 or Top-less was ectopically expressed. As seen in Figure 4D, the amount of t-loops is

It is unlikely that the effect of TRF2 knockdown on telomere DNA topology is related to a decrease in nucleosome occupancy, since we rather observe more H3 binding in this condition than when TRF2 is ectopically expressed (Figure S4C), in agreement with previous reports (Benetti et al., 2008; Galati et al., 2012), showing that Top-less is not impaired in at least some of the chromatin-remodeling properties of TRF2.

The topological change due to TRF2 dysfunction could be due to the increase in telomere transcription that was previously observed upon TRF2 depletion (Porro et al., 2014a, 2014b). However, Top-less fully rescues the increased TERRA expression observed in TRF2-compromised cells (Figures S5F and S5G).

Two facts suggested that Top-less could lead to variations in the t-loop content in cells: (1) the reduced capacity of this mutant to stimulate single-strand invasion in vitro (Figure 3C), a property thought to be involved in t-loop formation; (2) the telomere topological change caused by this mutant that could be linked to a loss of constraining structures such as t-loops. In order to investigate this, we performed direct stochastic optical reconstruction microscopy (STORM) imaging as described by Doksani et al. (2013). In order to increase our chances to observe t-loops, we used HT1080 cells overexpressing telomerase which can harbor telomeres of more than 20 kb (Cristofari and Lingner, 2006). Endogenous TRF2 expression was reduced by transfection of a siRNA directed against TRF2, and wild-type TRF2 or Top-less was ectopically expressed. As seen in Figure 4D, the amount of t-loops is

markedly decreased in Top-less cells as compared to wild-type TRF2 cells.

TRF2-Mediated DNA Wrapping Inhibits ATM Signaling

Next, we investigated DDR activation in the HeLa cell-line system used for Trioxsalen experiments (DOX-inducible expression of sh*TERF2*, lentiviral expression of TRF2, or Top-less). We scored telomere dysfunction-induced foci (TIFs) observed through the recruitment of 53BP1 on telomeres. As expected, knockdown of TRF2 significantly increased TIFs (Takai et al., 2003; Figure 5A). This telomere deprotection is rescued by exogenous expression of TRF2, but not of Top-less. Monitoring phosphorylated ATM (pATM) gave similar results, showing that Top-less is impaired in ATM inhibition (Figure S6A). In agreement, the CHK2 phosphorylation triggered by TRF2 downregulation is not fully rescued by Top-less expression (Figure S6B). Of note, in the time frame of our experiment, we could not detect modifications of the cell cycle (Figure S6C) ruling out an indirect effect of Top-less on cell proliferation. DDR activation was also observed in other Top-less-expressing cells (HT1080 supertelomerase cells used for t-loops measurements, BJ-HELT cells and HT1080 cells; Figures S6D, S6E, and S6F, respectively). We also observed an increased level of TIFs in cells expressing AΔB, a TRF2 mutant also compromised for DNA wrapping but through addition of the TRF1 acidic domain and not through TRFH mutations (as in Top-less) (Poulet et al., 2012).

We also analyzed this response in HT1080 cells by monitoring the colocalization of TRF1 and phosphorylated histone H2AX (γ H2AX). Again, we obtained a similar response for the Top-less mutant (Figure 5B). Of note, the expression of the 7K and 2R mutants in this setting rescued the telomere uncapping triggered by TRF2 inhibition. We concluded that the strong DDR activation at telomeres triggered by Top-less stems from the combination of both the 7K and 2R mutation sets.

We also explored whether Top-less could alter telomere length and cause formation of t-circles by 2D gel analysis. We did not observe overt production of t-circles and found no difference in mean telomere length upon TRF2 or Top-less expression (Figures S6G and S6H), suggesting that the decrease in t-loop number that we observed does not originate from t-loop excision. Finally, we measured the amount of the 3' overhang using an in-gel assay. As expected, TRF2 knockdown decreases the amount of 3' overhang, an effect rescued by both TRF2 and Top-less expression (Figure S6I), indicating that the decrease in t-loop formation is not caused by a decreased length of the 3' overhang.

In summary, the DNA-wrapping activity of TRF2 is required for telomere protection against ATM activation but is involved neither in telomere length regulation nor in 3' overhang formation.

TRF2-Mediated DNA Wrapping Inhibits NHEJ in RAP1-Compromised Cells

Then, we tested the ability of Top-less to prevent NHEJ by scoring telomere fusions in metaphase chromosomes. Upon TRF2 knockdown in HeLa cells, more than 20% of telomeres were fused (Figures 6A and 6B). This effect was rescued by both TRF2 and Top-less expression. Since RAP1 was previously shown to inhibit NHEJ independently of TRF2 (Bae and Bau-

mann, 2007; Sarthy et al., 2009), we analyzed the effect of Top-less in RAP1-compromised cells. In agreement with previous reports showing that RAP1 is dispensable for NHEJ protection in mammalian cells (Kabir et al., 2014), reducing its expression did not increase fusions in wild-type TRF2-expressing cells (Figures 6C and 6D). However, a 10-fold increase in the percentage of chromosome fusions was observed in Top-less cells upon RAP1 inhibition. This effect was rescued by an ectopic expression of RAP1, excluding an off-target effect of the RAP1 shRNA. These results indicate that TRF2-mediated DNA wrapping is involved in NHEJ inhibition independently of RAP1. Moreover, they reveal the anti-NHEJ activity of RAP1 as a backup mechanism for telomere protection in Top-less cells.

DISCUSSION

Although control of DNA topology is crucial for chromosomal integrity (Vos et al., 2011), our understanding of its role at telomeres is limited. Theoretically, the free DNA ends of telomeres should allow dissipation of torsional strain. The fact that we (Biroccio et al., 2011; Chen et al., 2015; Leonetti et al., 2008; Temime-Smaali et al., 2008; Ye et al., 2010) and others (d'Alcontres et al., 2014; Germe et al., 2009; Hsieh et al., 2015) have found that telomere integrity is particularly sensitive to topological stress suggests that telomeres may form topologically constrained chromatin entities. In agreement with this idea, telomeres harbor t-loop structures that may constitute topological barriers. In this report, we unveil that telomeres are topological objects that rely on a particular DNA-wrapping activity of TRF2 to be protected against ATM activation and NHEJ.

By combining AFM, DREEM, protein footprinting, and topology assays, we demonstrate that 90 bp of DNA wrap around the TRFH domain of TRF2 through an interaction with a set of lysines and arginines located on the surface of this domain. Interestingly, the localization of these residues on the TRFH domain imposes a chirality in the DNA-TRF2 complex (Figure S2D).

The identification of TRFH residues contacting DNA allowed us to design a mutant largely deficient in wrapping activity and therefore named Top-less. Top-less behaves as a valuable separation-of-function mutant to study the role of DNA topology at telomeres since, on one hand, it alters the topological state of telomeric DNA *in vitro* and *in vivo*, while on another hand, it conserves many TRF2 properties, including (1) proper folding according to CD analysis, (2) specific binding to telomeric DNA both *in vitro* and *in vivo*, (3) TIN2 and RAP1 recruitment at telomeres, (4) facilitation of Holliday junction formation and inhibition of their migration, and (5) unaltered expression of the other shelterin subunits.

Top-less causes a marked ATM activation at telomeres showing a loss of function for ATM inhibition. Of note, the parental mutants 7K and 2R, which bear separately the seven mutated lysines (7K) or the two arginines (2R) mutated in Top-less, fully protect against ATM activation. Moreover, the wrapping-deficient AΔB mutant, bearing a wild-type TRFH domain, behaves similarly to Top-less *in vivo*. Overall, the behavior of these mutants indicates that Top-less-mediated telomere deprotection is not due to alterations in unidentified TRFH binding sites for cellular factors. Of note, Top-less cells not only recruit

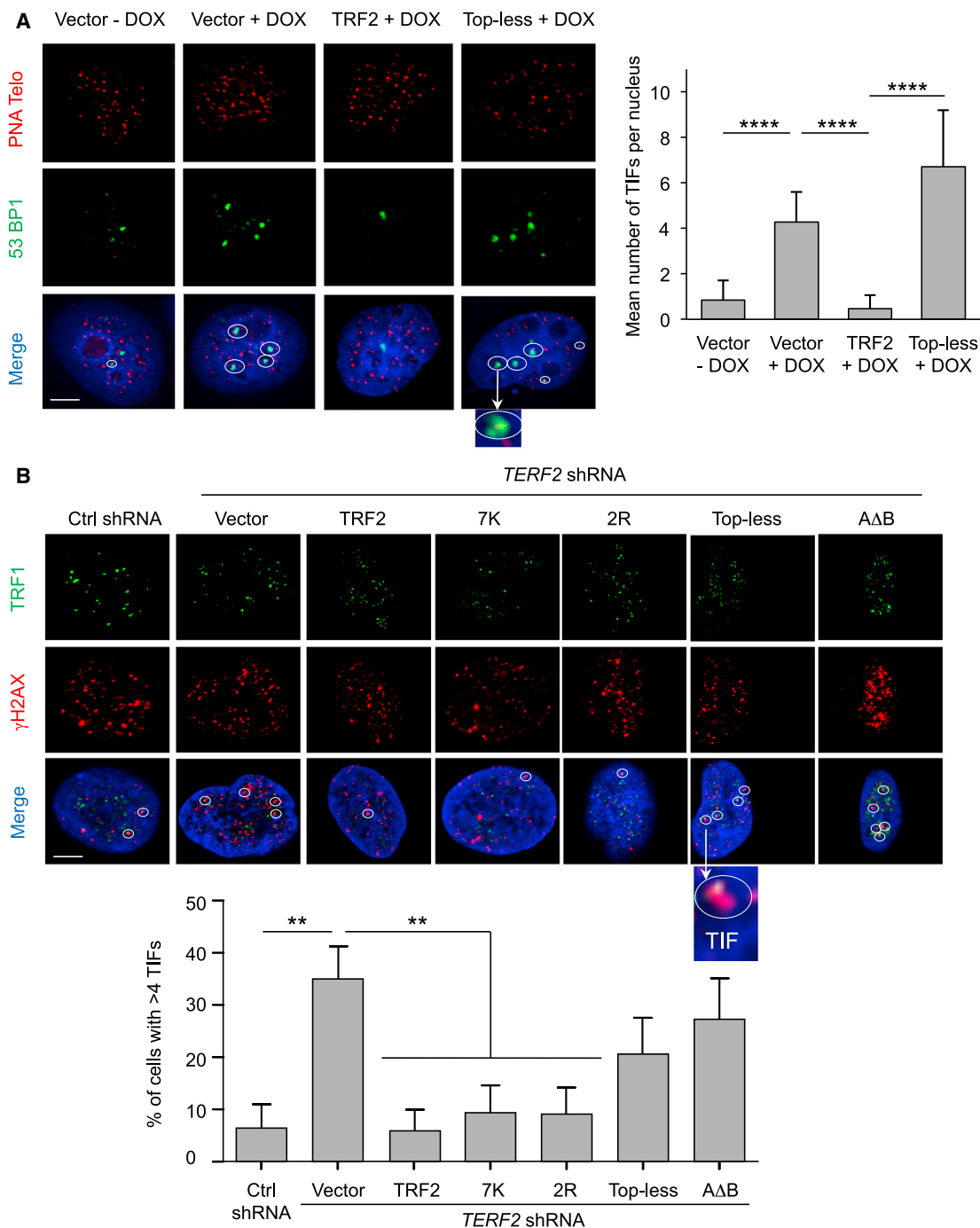


Figure 5. Top-less Does Not Protect against DDR Activation

(A) (Left) Representative section images of detection of 53BP1 by IF (green), telomeric DNA (red), and the merge with DAPI (blue) under the indicated conditions. TIFs are marked with a circle. Scale bar, 5 μ m.

(Right) TIFs per nucleus were quantified. Data represent the means \pm SE. p values were calculated using the Mann-Whitney test (****p < 0.0001).

(B) (Top) Representative section images of detection of TRF1 by IF (green), γ -H2AX by IF (red), and the merge with DAPI (blue) under the indicated conditions using HT1080 cells. TIFs are marked circles. Scale bar, 5 μ m.

(Bottom) The percentage of cells showing more than four TIFs was quantified. Data represent the means \pm SE. p values were calculated using the Mann-Whitney test (**p < 0.01; absence of mark indicates no significance). The quantification of *TERF2* transcript level for the different conditions (control scramble shRNA with expression of empty vector, *TERF2* shRNA with expression of either empty vector or TRF2, 7K, 2R, Top-less, or AΔB) was done by RT-qPCR and is, respectively, 1, 0.65, 20, 42, 76, 41.

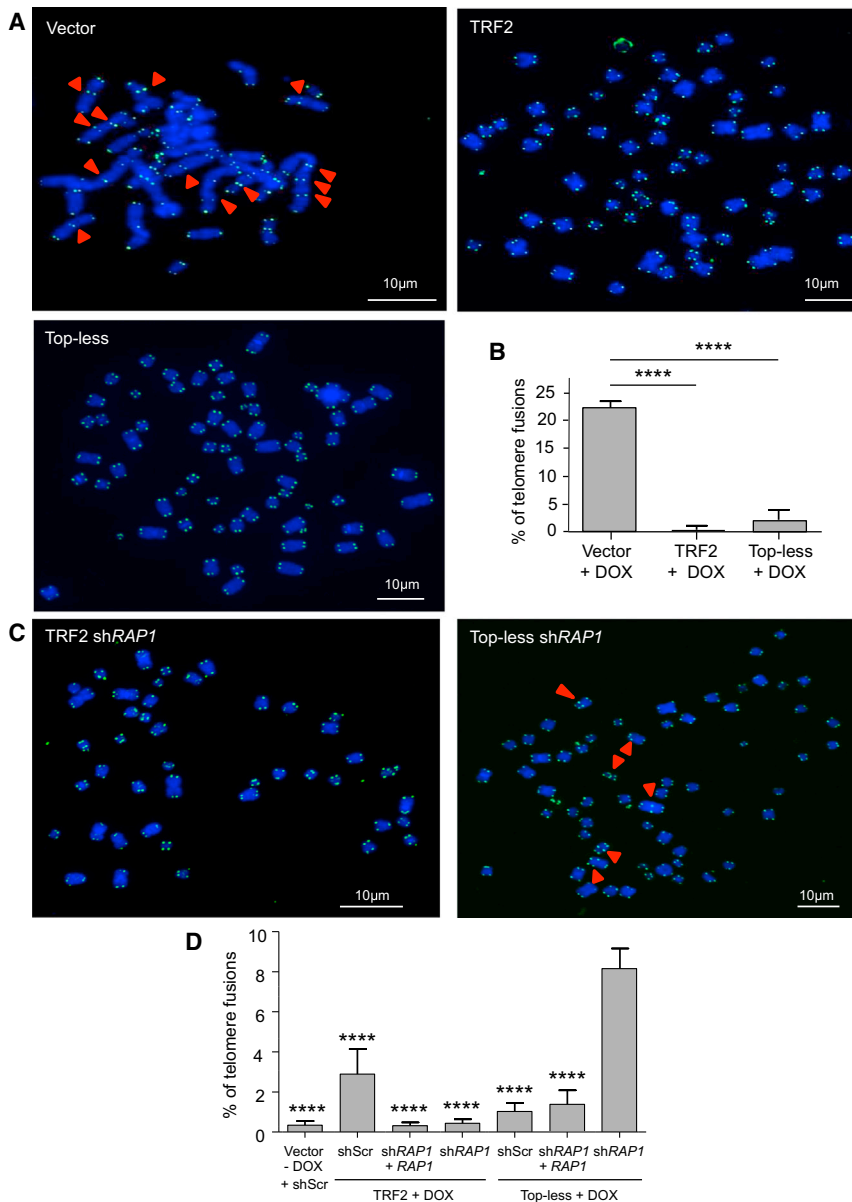


Figure 6. TRF2-Mediated DNA Wrapping Inhibits NHEJ in RAP1-Compromised Cells

(A) Metaphase chromosome spreads of HeLa cells transduced with either empty vector, TRF2, or Top-less viruses upon TRF2 knockdown using doxycycline (DOX). Chromosomes were stained for telomeric DNA (green) and with DAPI (blue). The red arrows show examples of telomere fusions. (B) Graph showing the percentage of fusions counted on 2,000 chromosomes. Data represent the means \pm SE, and p values were calculated using Student's t test (****p < 0.0001; absence of a mark indicates no significance).

(C) Metaphase chromosome spreads of HeLa cells transduced with TRF2 or Top-less viruses upon TRF2 knockdown using doxycycline (DOX) and knockdown of RAP1 by shRNA.

(D) Graph showing the percentage of fusions counted on 2,000 chromosomes for each condition. p value was calculated using a one-way ANOVA (****p < 0.0001). Downregulation of *RAP1* was quantified by RT-qPCR and corresponded to a knockdown of 83%.

fact that Top-less is unable to facilitate strand invasion, a key mechanism in t-loop formation (Griffith et al., 1999). As an explanation, DNA wrapping around the TRFH domain could be involved in strand invasion and t-loop folding through the unwinding of DNA outside TRF2 binding sites as we suggested earlier (Amiard et al., 2007). The efficient protection against telomere fusion in Top-less cells seems contradictory to the previously proposed protective role of t-loops against NHEJ (Doksani et al., 2013). Since mammalian RAP1 was shown to protect against NHEJ in a TRF2-independent manner (Bae and Baumann, 2007; Sarthy et al., 2009) and Top-less can still recruit RAP1 at telomeres, RAP1 could provide a backup anti-NHEJ mechanism in Top-less cells (Figure 6E). Indeed, a reduced

phosphorylated ATM and γ -H2AX at telomeres but also recruit 53BP1. Together with an increased amount of phosphorylated CHK2, these results show that Top-less telomeres are impaired in the inhibition of both the initiation and the propagation of ATM signaling. This might appear at odds with the preservation in Top-less of a small region of the hinge domain (iDDR domain, aa 407–431), which has been shown to inhibit the recruitment of 53BP1 (Okamoto et al., 2013). One explanation to reconcile these results could be that the iDDR domain function is somehow altered by the Top-less mutations. In agreement, the iDDR domain lies in a region where the lysine acetylation profile changes upon DNA binding (Figure 2A).

An important result of this study is that Top-less cells exhibit a decreased number of t-loops, indicating that TRF2-wrapping activity is required for t-loop folding. This is in agreement with the

expression of RAP1 triggers a marked increase in telomere fusions in Top-less. These results show that TRF2 can protect against NHEJ through different mechanisms, including the recruitment at telomeres of RAP1 and its capacity to wrap DNA around its TRFH domain.

Our results show that one of the mechanisms by which telomeres control their DNA topology and protect against ATM activation and NHEJ stems from the right-handed wrapping of telomeric DNA around the TRFH domain of TRF2. Three independent findings support this conclusion: (1) TRF2 wraps DNA in a right-handed manner, (2) TRF2 controls telomere DNA topology in human cells, and (3) the expression of TRF2 mutants specifically impaired in this wrapping activity fails to control telomere DNA topology and uncaps telomeres. Several nonexclusive mechanisms can be envisaged

to link the topological properties of TRF2 to ATM signaling and NHEJ. One is suggested by the decreased amount of t-loops in Top-less cells. This is in agreement with the view that t-loops prevent ATM activation and constitute a poor substrate for NHEJ. Another, nonexclusive possibility is that TRF2 acts as a torsional strain sensor to orchestrate various activities required to resolve topological problems that may arise during DNA processing (replication, transcription, and repair).

In RAP1-proficient cells, Top-less uncouples ATM inhibition from the anti-NHEJ activity of TRF2. Interestingly, this partially uncapped telomere phenotype of Top-less cells is reminiscent of the phenotype of cells either exhibiting spontaneous DDR activation at telomeres (Cesare et al., 2009; Kaul et al., 2012; Thanasoula et al., 2010), either with a reduced expression of TRF2 (Cesare et al., 2013), either upon prolonged mitotic arrest (Hayashi et al., 2012) or upon deletion of the *TIN2* gene (Takai et al., 2011). This phenotype is described as an “intermediate state” of telomere protection and was proposed to occur when telomeres of primary human cells become too short to efficiently protect against DDR activation and to lead to cell senescence (Cesare and Karlseder, 2012). A topology switch at telomeres may thus constitute a common mechanism leading to the appearance of such intermediate state telomeres. In this hypothesis, our results predict that RAP1 may be critical to protect telomeres of senescent cells from NHEJ.

This study reveals that telomeres directly use positively superhelical strain to escape from inappropriate activation of DDR. Such a functional link between telomere DNA topology and DDR control is reminiscent of the transcription of nuclear pore-associated genes in yeast (Bermejo et al., 2011). The involvement of mechanisms that control DNA topology in telomeric functions appears conserved during evolution since bacteria and yeast telomeres also rely on topoisomerase to maintain their integrity (Bankhead et al., 2006; Bao and Cohen, 2004; Chaconas and Kobryn, 2010; Germe et al., 2009; Mirabella and Gartenberg, 1997; Tsai et al., 2011). Thus, we propose that the folding of telomeres into topologically constrained superstructures is a universal feature of telomeres that may have been used as a mechanism for end protection during chromosome evolution.

EXPERIMENTAL PROCEDURES

Only specific techniques used in this study are presented in this section. Published protocols have been used for several experiments and are detailed in the [Supplemental Information](#).

Proteins

All proteins were obtained using the plasmid pTrcHisB (Invitrogen), bearing an N-terminal His-tag fusion, and were produced from DH5 α bacteria, as described (Poulet et al., 2012). The TRF2 protein used corresponds to a 500 aa peptide.

Cell Lines and Reagents

HT1080 cells were grown in DMEM supplemented with 10% fetal calf serum, penicillin (100 IU/ml), and streptomycin (100 μ g/ml) at 37°C. sh*TERF2*-inducible HeLa cells were a gift from Joachim Lingner and were used as described previously (Grolimund et al., 2013).

The sequence of *TERF2* shRNA used in HT1080 cells was 5'-CCGGCAT TGGAAATGATGACTCTGAACTCGAGTTCAGAGTCATCATTCCAATGTTTTT-3'. Lentivirus production was performed by transient cotransfection of 293T cells with the specified lentiviral-expression vector and two packaging plasmids, p8.91 and pVSVg, by calcium-phosphate precipitation. Viral supernatants were collected 24 hr after transfection. The transduction efficiency was determined for the pWPIR-GFP vectors (pWPIR-GFP, pWPIR-GFP-TRF2, pWPIR-GFP-7K, pWPIR-GFP-2R, pWPIR-GFP-Top-less, and pWPIR-GFP- Δ AB) by flow-cytometry analysis of GFP-positive cells 3 days after infection and for the pLKO-shRNA plasmids (pLKO-shScramble and pLKO-sh*TERF2*) by counting the number of clones after 1 week of selection with puromycin (1 μ g/ml).

DREEM Imaging

Topographic signals are collected through mechanically driving cantilevers near its resonance frequency. Simultaneously, electrostatic signals are collected through applying AC and DC biases to a highly doped silicon cantilever with the frequency of the AC bias centered on cantilever's first overtone. Importantly, there are no significant cross-talks between topographic and DREEM channels. The DNA substrates were a mixture of DNA (T135 DNA) fragments from digestion of the pSXneo 135 (T2AG3) plasmid DNA (a gift from Dr. Peter Lansdorp at the University of British Columbia) using XbaI and BglII restriction enzymes (NEB). The two fragments resulted from digestion and have distinct DNA contour lengths, which enable us to differentiate telomeric (263 nm) and plasmidic (1,150 nm) DNA fragments. The TRFH domain was diluted to a final concentration of 445 nM in 5 mM HEPES, 150 mM KCl (pH 7.5) and incubated with the T135 DNA fragments (2 nM) for 20 min at room temperature. The incubated samples were diluted 20-fold in 5 mM HEPES, 150 mM KCl, 10 mM Mg(OAc)₂ (pH 7.5) and deposited onto freshly cleaved mica surface (SPI Supply). DREEM images were collected using a MFP-3D-Bio AFM (Asylum Research) and highly doped Pointprobe PPP-FMR probes (Nanosensors; results for force constant were as follows: \sim 2.8 N/m; results for resonant frequency were as follows: $f_1 = \sim$ 80 kHz; and results for first overtone were as follows: $f_2 \sim$ 500 kHz). Detailed description of DREEM imaging technique is described in two studies (K.P., D. Wu, J. Lin, P. Countryman, R. Riehn, P.L. Opreško, and H. Wang, unpublished data; Wu et al., 2016). Briefly, AFM cantilevers were scraped with tweezers to remove the oxidized layer, and the top surface was coated with a thin layer of colloidal liquid silver (Ted Pella Inc.). A function generator (Sanford Research System, model DS335) and lock-in amplifier (Sanford Research System, model SR844 RF) were used to generate the AC and DC biases and monitor changes in vibration amplitude and phase signals near the first overtone frequency as a function of sample positions. While the AC and DC biases are applied to AFM tips, the mica substrate is grounded. To optimize DREEM signals, AC and DC biases were adjusted from 0 to 20 V and -1.5 to 1.5 V, respectively.

Protein Footprinting

In total, 8 pmol of TRF2 protein were incubated for 20 min at 25°C with or without 16 pmol of a linearized DNA plasmid containing 650 bp of telomeric sequences in 10 mM Tris-HCl (pH 8), 150 mM NaCl, 0.5 mM DTT, and 5% glycerol. Acetylation of lysines was performed by adding 0.5 mM of sulfo-succinimidyl acetate (Thermo scientific) for 30 min at 30°C. The reaction was stopped by adding 1% trifluoroacetic acid (Sigma). The samples were resuspended in Laemmli loading buffer and boiled for 5 min. Proteins were resolved by SDS-PAGE and submitted to trypsin proteolysis, and profiles of lysine acetylation were analyzed using mass spectrometry. We determined the probability of lysine acetylation and the probability of disappearance of lysine acetylation upon DNA interaction. The percentage of protection from acetylation presented in [Figure 2](#) was calculated as follows: probability of disappearance of lysine acetylation upon DNA interaction \times probability of lysine acetylation of the TRF2 protein. Data shown are the results of five independent experiments.

Trioxsalen Experiments

In total, two million HeLa cells were treated with or without doxycycline (1 μ g/ml for 5 days) and ICRF-193 (3 μ g/ml final concentration for 24 hr)

and transduced by the Empty, TRF2, or Top-less expressing vectors. Treatment was performed in a 10 cm Petri dish in PBS with 280 μ l of a saturated 0.9 mg/ml solution of 4,5',8-trimethylpsoralen (Trioxsalen) for 4 min at 37°C in aluminum foil. Crosslinking was performed on a BioSun (Vilber Lourmat) at 350 nm at 0.36 J/cm². Then, trioxsalen was removed and cells were washed, trypsinized, and pelleted. After classical extraction, DNA was resuspended in 75 μ l of TE and sonicated using a Bioruptor (Diagenode) until fragments were around 200 bp in length. This length was checked using a Bioanalyzer (Agilent). A total of 8 μ g of DNA was dried using a speed vac, resuspended in 10 μ l of Glyoxal buffer (1 M Glyoxal, 50% DMSO), and incubated at 55°C for 90 min. Orange dye loading buffer was added, and samples were loaded on a 3% agarose 10 mM Na phosphate buffer (pH 7) gel. Migration was performed for 14 hr in 10 mM Na phosphate buffer (pH 7) at 2.5 V/cm. After migration, the gel was incubated for 3 hr at 65°C in 0.5 N NaOH and 1.5 M NaCl. After several washes in water, the gel was incubated 3 times for 20 min in 1 \times TBE, and 40 μ l of SYBR Green II (Life Technologies) was added to 200 μ l of 1 \times TBE for staining. After rinsing with water, the gel was scanned using a Typhoon FLA 9500 (GE Healthcare). DNA in the gel was then transferred to a N+ Hybond membrane (Southern blotting), telomeric DNA was revealed using a telomeric radiolabeled probe, and the membrane was analyzed as for EMSA gels.

SUPPLEMENTAL INFORMATION

Supplemental Information includes Supplemental Experimental Procedures and six figures and can be found with this article online at <http://dx.doi.org/10.1016/j.molcel.2015.12.009>.

AUTHOR CONTRIBUTIONS

D.B.-P. performed cell biology and microscopy experiments with the help of E.J., K.F., S.B., N.D., C.M.L., S.P., A.M.-B., and J.Y.; S.P. performed AFM and STORM with the assistance of V.F., A.L.-V., and S.B.; D.B.-P., A.M.-B., L.L., and M.-J.G.-P. did the biochemical analysis of biological samples; D.B.-P., B.P., A.G., and M.-J.G.-P. performed in vitro biochemical experiments; S.M. and M.-H.L. conducted CD. E.A. constructed the HeLa cell line. P.K. and H.W. performed DREEM experiments. J.C.-V. assisted for data analysis. D.B.-P. and S.P. were involved in the writing of the manuscript. E.G. and M.-J.G.-P. coordinated the study and wrote the manuscript.

ACKNOWLEDGMENTS

We greatly thank Joachim Lingner for the HeLa cell line used in this study. This work was performed using the genomic, PICMI (supported by ARC and the Conseil General 06 de la Région Provence Alpes-Côte d'Azur), and CYTOMED (supported by FEDER, le Ministère de l'Enseignement Supérieur, la région Provence Alpes-Côte d'Azur, and l'INSERM) facilities of IR-CAN; we are very grateful for the help they provided. We are also indebted to Isabelle Zanella-Cléon for mass spectrometry analysis (Centre Commun de Micro-analyse des Protéines, IBCP Lyon). We acknowledge the PICT-IBiSA platform of the Institut Curie, member of the French National Research Infrastructure France-Bioluming (ANR-10-INSB-04). We are grateful to Matteo de Chiara and Silvia Bottini for the script of 2D probability density map on R. The AFM facility of PICMI was supported by the ARC and Conseil General 06 de la Région Provence Alpes-Côte d'Azur. This work was supported by grants from the Fondation ARC, Ligue Contre le Cancer (EG Equipe labellisée), ANR ("Teloloop" ANR-1582-30020690), Institut Nationale du Cancer (INCa) (TELOCHROM), "Investments for the Future" LABEX SIGNALIFE (reference ANR-11-LABX-0028-01), and an NIH grant for DREEM experiments (NIH R01GM107559).

Received: June 8, 2015

Revised: October 14, 2015

Accepted: November 30, 2015

Published: January 7, 2016

REFERENCES

- Amiard, S., Doudeau, M., Pinte, S., Poulet, A., Lenain, C., Fèvre-Moskalenko, C., Angelov, D., Hug, N., Vindigni, A., Bouvet, P., et al. (2007). A topological mechanism for TRF2-enhanced strand invasion. *Nat. Struct. Mol. Biol.* **14**, 147–154.
- Bae, N.S., and Baumann, P. (2007). A RAP1/TRF2 complex inhibits nonhomologous end-joining at human telomeric DNA ends. *Mol. Cell* **26**, 323–334.
- Baker, A.M., Fu, Q., Hayward, W., Lindsay, S.M., and Fletcher, T.M. (2009). The Myb/SANT domain of the telomere-binding protein TRF2 alters chromatin structure. *Nucleic Acids Res.* **37**, 5019–5031.
- Baker, A.M., Fu, Q., Hayward, W., Victoria, S., Pedrosa, I.M., Lindsay, S.M., and Fletcher, T.M. (2011). The telomere binding protein TRF2 induces chromatin compaction. *PLoS ONE* **6**, e19124.
- Bankhead, T., Kobryn, K., and Chaconas, G. (2006). Unexpected twist: harnessing the energy in positive supercoils to control telomere resolution. *Mol. Microbiol.* **62**, 895–905.
- Bao, K., and Cohen, S.N. (2004). Reverse transcriptase activity innate to DNA polymerase I and DNA topoisomerase I proteins of *Streptomyces* telomere complex. *Proc. Natl. Acad. Sci. USA* **101**, 14361–14366.
- Benetti, R., Schoeftner, S., Muñoz, P., and Blasco, M.A. (2008). Role of TRF2 in the assembly of telomeric chromatin. *Cell Cycle* **7**, 3461–3468.
- Bermejo, R., Capra, T., Jossen, R., Colosio, A., Frattini, C., Carotenuto, W., Cocito, A., Doksan, Y., Klein, H., Gómez-González, B., et al. (2011). The replication checkpoint protects fork stability by releasing transcribed genes from nuclear pores. *Cell* **146**, 233–246.
- Bilaud, T., Koering, C.E., Binet-Brasselet, E., Ancelin, K., Pollice, A., Gasser, S.M., and Gilson, E. (1996). The telobox, a Myb-related telomeric DNA binding motif found in proteins from yeast, plants and human. *Nucleic Acids Res.* **24**, 1294–1303.
- Bilaud, T., Brun, C., Ancelin, K., Koering, C.E., Laroche, T., and Gilson, E. (1997). Telomeric localization of TRF2, a novel human telobox protein. *Nat. Genet.* **17**, 236–239.
- Biroccio, A., Porru, M., Rizzo, A., Salvati, E., D'Angelo, C., Orlandi, A., Passeri, D., Franceschin, M., Stevens, M.F., Gilson, E., et al. (2011). DNA damage persistence as determinant of tumor sensitivity to the combination of Topo I inhibitors and telomere-targeting agents. *Clin Cancer Res* **17**, 2227–2236.
- Celli, G.B., and de Lange, T. (2005). DNA processing is not required for ATM-mediated telomere damage response after TRF2 deletion. *Nat. Cell Biol.* **7**, 712–718.
- Cesare, A.J., and Karlseder, J. (2012). A three-state model of telomere control over human proliferative boundaries. *Curr. Opin. Cell Biol.* **24**, 731–738.
- Cesare, A.J., Kaul, Z., Cohen, S.B., Napier, C.E., Pickett, H.A., Neumann, A.A., and Reddel, R.R. (2009). Spontaneous occurrence of telomeric DNA damage response in the absence of chromosome fusions. *Nat. Struct. Mol. Biol.* **16**, 1244–1251.
- Cesare, A.J., Hayashi, M.T., Crabbe, L., and Karlseder, J. (2013). The telomere deprotection response is functionally distinct from the genomic DNA damage response. *Mol. Cell* **51**, 141–155.
- Chaconas, G., and Kobryn, K. (2010). Structure, function, and evolution of linear replicons in *Borrelia*. *Annu. Rev. Microbiol.* **64**, 185–202.
- Chen, Y., Yang, Y., van Overbeek, M., Donigian, J.R., Baci, P., de Lange, T., and Lei, M. (2008). A shared docking motif in TRF1 and TRF2 used for differential recruitment of telomeric proteins. *Science* **319**, 1092–1096.
- Chen, L., Zhu, X., Zou, Y., Xing, J., Gilson, E., Lu, Y., and Ye, J. (2015). The topoisomerase II catalytic inhibitor ICRF-193 preferentially targets telomeres that are capped by TRF2. *Am. J. Physiol. Cell Physiol.* **308**, C372–C377.
- Court, R., Chapman, L., Fairall, L., and Rhodes, D. (2005). How the human telomeric proteins TRF1 and TRF2 recognize telomeric DNA: a view from high-resolution crystal structures. *EMBO Rep.* **6**, 39–45.
- Cristofari, G., and Lingner, J. (2006). Telomere length homeostasis requires that telomerase levels are limiting. *EMBO J.* **25**, 565–574.

- d'Alcontres, M.S., Palacios, J.A., Mejias, D., and Blasco, M.A. (2014). Topoliz prevents telomere fragility and formation of ultra thin DNA bridges during mitosis through TRF1-dependent binding to telomeres. *Cell Cycle* **13**, 1463–1481.
- de Lange, T. (2005). Shelterin: the protein complex that shapes and safeguards human telomeres. *Genes Dev.* **19**, 2100–2110.
- Denchi, E.L., and de Lange, T. (2007). Protection of telomeres through independent control of ATM and ATR by TRF2 and POT1. *Nature* **448**, 1068–1071.
- Doksani, Y., Wu, J.Y., de Lange, T., and Zhuang, X. (2013). Super-resolution fluorescence imaging of telomeres reveals TRF2-dependent T-loop formation. *Cell* **155**, 345–356.
- Fairall, L., Chapman, L., Moss, H., de Lange, T., and Rhodes, D. (2001). Structure of the TRFH dimerization domain of the human telomeric proteins TRF1 and TRF2. *Mol. Cell* **8**, 351–361.
- Feuerhahn, S., Chen, L.Y., Luke, B., and Porro, A. (2015). No DDRama at chromosome ends: TRF2 takes centre stage. *Trends Biochem. Sci.* **40**, 275–285.
- Fouché, N., Cesare, A.J., Willcox, S., Ozgür, S., Compton, S.A., and Griffith, J.D. (2006). The basic domain of TRF2 directs binding to DNA junctions irrespective of the presence of TTAGGG repeats. *J. Biol. Chem.* **281**, 37486–37495.
- Galati, A., Magdinier, F., Colasanti, V., Bauwens, S., Pinte, S., Ricordy, R., Giraud-Panis, M.J., Pusch, M.C., Savino, M., Cacchione, S., and Gilson, E. (2012). TRF2 controls telomeric nucleosome organization in a cell cycle phase-dependent manner. *PLoS ONE* **7**, e34386.
- Germe, T., Miller, K., and Cooper, J.P. (2009). A non-canonical function of topoisomerase II in disentangling dysfunctional telomeres. *EMBO J.* **28**, 2803–2811.
- Gilson, E., and Géli, V. (2007). How telomeres are replicated. *Nat. Rev. Mol. Cell Biol.* **8**, 825–838.
- Giraud-Panis, M.J., Pisano, S., Benarroch-Popivker, D., Pei, B., Le Du, M.H., and Gilson, E. (2013). One identity or more for telomeres? *Front. Oncol.* **3**, 48.
- Griffith, J.D., Comeau, L., Rosenfield, S., Stansel, R.M., Bianchi, A., Moss, H., and de Lange, T. (1999). Mammalian telomeres end in a large duplex loop. *Cell* **97**, 503–514.
- Grolimund, L., Aeby, E., Hamelin, R., Armand, F., Chiappe, D., Moniatte, M., and Lingner, J. (2013). A quantitative telomeric chromatin isolation protocol identifies different telomeric states. *Nat. Commun.* **4**, 2848–2859.
- Hayashi, M.T., Cesare, A.J., Fitzpatrick, J.A., Lazzerini-Denchi, E., and Karlseder, J. (2012). A telomere-dependent DNA damage checkpoint induced by prolonged mitotic arrest. *Nat. Struct. Mol. Biol.* **19**, 387–394.
- Hsieh, M.H., Tsai, C.H., Lin, C.C., Li, T.K., Hung, T.W., Chang, L.T., Hsin, L.W., and Teng, S.C. (2015). Topoisomerase II inhibition suppresses the proliferation of telomerase-negative cancers. *Cell. Mol. Life Sci.* **72**, 1825–1837.
- Kabir, S., Hockemeyer, D., and de Lange, T. (2014). TALEN gene knockouts reveal no requirement for the conserved human shelterin protein Rap1 in telomere protection and length regulation. *Cell Rep.* **9**, 1273–1280.
- Kaul, Z., Cesare, A.J., Huschtscha, L.I., Neumann, A.A., and Reddel, R.R. (2012). Five dysfunctional telomeres predict onset of senescence in human cells. *EMBO Rep.* **13**, 52–59.
- Kim, H., Lee, O.H., Xin, H., Chen, L.Y., Qin, J., Chae, H.K., Lin, S.Y., Safari, A., Liu, D., and Songyang, Z. (2009). TRF2 functions as a protein hub and regulates telomere maintenance by recognizing specific peptide motifs. *Nat. Struct. Mol. Biol.* **16**, 372–379.
- Kouzine, F., Gupta, A., Baranello, L., Wojtowicz, D., Ben-Aissa, K., Liu, J., Przytycka, T.M., and Levens, D. (2013). Transcription-dependent dynamic supercoiling is a short-range genomic force. *Nat. Struct. Mol. Biol.* **20**, 396–403.
- Leonetti, C., Scarsella, M., Riggio, G., Rizzo, A., Salvati, E., D'Incalci, M., Staszewsky, L., Frapolli, R., Stevens, M.F., Stoppacciaro, A., et al. (2008). G-quadruplex ligand RHPS4 potentiates the antitumor activity of camptothecins in preclinical models of solid tumors. *Clin Cancer Res* **14**, 7284–7291.
- Mendoza, V.L., and Vachet, R.W. (2009). Probing protein structure by amino acid-specific covalent labeling and mass spectrometry. *Mass Spectrom. Rev.* **28**, 785–815.
- Mirabella, A., and Gartenberg, M.R. (1997). Yeast telomeric sequences function as chromosomal anchorage points in vivo. *EMBO J.* **16**, 523–533.
- Muraki, K., Nabetani, A., Nishiyama, A., and Ishikawa, F. (2011). Essential roles of Xenopus TRF2 in telomere end protection and replication. *Genes Cells* **16**, 728–739.
- Okamoto, K., Bartocci, C., Ouzounov, I., Diedrich, J.K., Yates, J.R., 3rd, and Denchi, E.L. (2013). A two-step mechanism for TRF2-mediated chromosome-end protection. *Nature* **494**, 502–505.
- Porro, A., Feuerhahn, S., Delafontaine, J., Riethman, H., Rougemont, J., and Lingner, J. (2014a). Functional characterization of the TERRA transcriptome at damaged telomeres. *Nat. Commun.* **5**, 5379–5391.
- Porro, A., Feuerhahn, S., and Lingner, J. (2014b). TERRA-reinforced association of LSD1 with MRE11 promotes processing of uncapped telomeres. *Cell Rep.* **6**, 765–776.
- Poulet, A., Buisson, R., Faivre-Moskalenko, C., Koelblen, M., Amiard, S., Montel, F., Cuesta-Lopez, S., Bornet, O., Guerlesquin, F., Godet, T., et al. (2009). TRF2 promotes, remodels and protects telomeric Holliday junctions. *EMBO J.* **28**, 641–651.
- Poulet, A., Pisano, S., Faivre-Moskalenko, C., Pei, B., Tauran, Y., Haftek-Terreau, Z., Brunet, F., Le Bihan, Y.V., Ledu, M.H., Montel, F., et al. (2012). The N-terminal domains of TRF1 and TRF2 regulate their ability to condense telomeric DNA. *Nucleic Acids Res.* **40**, 2566–2576.
- Saint-Léger, A., Koelblen, M., Civitelli, L., Bah, A., Djerbi, N., Giraud-Panis, M.J., Londoño-Vallejo, A., Ascenzioni, F., and Gilson, E. (2014). The basic N-terminal domain of TRF2 limits recombination endonuclease action at human telomeres. *Cell Cycle* **13**, 2469–2474.
- Sarek, G., Vannier, J.B., Panier, S., Petrini, J.H., and Boulton, S.J. (2015). TRF2 recruits RTEL1 to telomeres in S phase to promote t-loop unwinding. *Mol. Cell* **57**, 622–635.
- Sarthy, J., Bae, N.S., Scraftford, J., and Baumann, P. (2009). Human RAP1 inhibits non-homologous end joining at telomeres. *EMBO J.* **28**, 3390–3399.
- Stansel, R.M., de Lange, T., and Griffith, J.D. (2001). T-loop assembly in vitro involves binding of TRF2 near the 3' telomeric overhang. *EMBO J.* **20**, 5532–5540.
- Takai, H., Smogorzewska, A., and de Lange, T. (2003). DNA damage foci at dysfunctional telomeres. *Curr. Biol.* **13**, 1549–1556.
- Takai, K.K., Kibe, T., Donigian, J.R., Frescas, D., and de Lange, T. (2011). Telomere protection by TPP1/POT1 requires tethering to TIN2. *Mol. Cell* **44**, 647–659.
- Temime-Smaali, N., Guittat, L., Wenner, T., Bayart, E., Douarre, C., Gomez, D., Giraud-Panis, M.J., Londoño-Vallejo, A., Gilson, E., Amor-Guérét, M., and Riou, J.F. (2008). Topoisomerase IIIalpha is required for normal proliferation and telomere stability in alternative lengthening of telomeres. *EMBO J.* **27**, 1513–1524.
- Thanasoula, M., Escandell, J.M., Martinez, P., Badie, S., Muñoz, P., Blasco, M.A., and Tarsounas, M. (2010). p53 prevents entry into mitosis with uncapped telomeres. *Curr. Biol.* **20**, 521–526.
- Tsai, H.H., Huang, C.H., Tessmer, I., Erie, D.A., and Chen, C.W. (2011). Linear *Streptomyces* plasmids form superhelical circles through interactions between their terminal proteins. *Nucleic Acids Res.* **39**, 2165–2174.
- van Steensel, B., Smogorzewska, A., and de Lange, T. (1998). TRF2 protects human telomeres from end-to-end fusions. *Cell* **92**, 401–413.
- Verdun, R.E., and Karlseder, J. (2006). The DNA damage recombination pathway act consecutively to protect human telomeres. *Cell* **127**, 709–720.

- Vos, S.M., Tretter, E.M., Schmidt, B.H., and Berger, J.M. (2011). All tangled up: how cells direct, manage and exploit topoisomerase function. *Nat. Rev. Mol. Cell Biol.* *12*, 827–841.
- Wan, B., Yin, J., Horvath, K., Sarkar, J., Chen, Y., Wu, J., Wan, K., Lu, J., Gu, P., Yu, E.Y., et al. (2013). SLX4 assembles a telomere maintenance toolkit by bridging multiple endonucleases with telomeres. *Cell Rep.* *4*, 861–869.
- Wilson, J.S., Tejera, A.M., Castor, D., Toth, R., Blasco, M.A., and Rouse, J. (2013). Localization-dependent and -independent roles of SLX4 in regulating telomeres. *Cell Rep.* *4*, 853–860.
- Wu, D., Kaur, P., Wang, H., and Erie, D.A. (2016). Visualizing the path of DNA through proteins using DREEM imaging. *Mol. Cell* *61*, this issue, 315–323.
- Ye, J., Lenain, C., Bauwens, S., Rizzo, A., Saint-Léger, A., Poulet, A., Benarroch, D., Magdinier, F., Morere, J., Amiard, S., et al. (2010). TRF2 and apollo cooperate with topoisomerase 2alpha to protect human telomeres from replicative damage. *Cell* *142*, 230–242.
- Yeeles, J.T., Poli, J., Marians, K.J., and Pasero, P. (2013). Rescuing stalled or damaged replication forks. *Cold Spring Harb. Perspect. Biol.* *5*, a012815.

Molecular Cell

Supplemental Information

TRF2-Mediated Control of Telomere DNA Topology

as a Mechanism for Chromosome-End Protection

Delphine Benarroch-Popivker, Sabrina Pisano, Aaron Mendez-Bermudez, Liudmyla Lototska, Parminder Kaur, Serge Bauwens, Nadir Djerbi, Chrysa M. Latrick, Vincent Fraasier, Bei Pei, Alexandre Gay, Emilie Jaune, Kevin Foucher, Julien Cherfils-Vicini, Eric Aeby, Simona Miron, Arturo Londoño-Vallejo, Jing Ye, Marie-Hélène Le Du, Hong Wang, Eric Gilson, and Marie-Josèphe Giraud-Panis

Figure S1

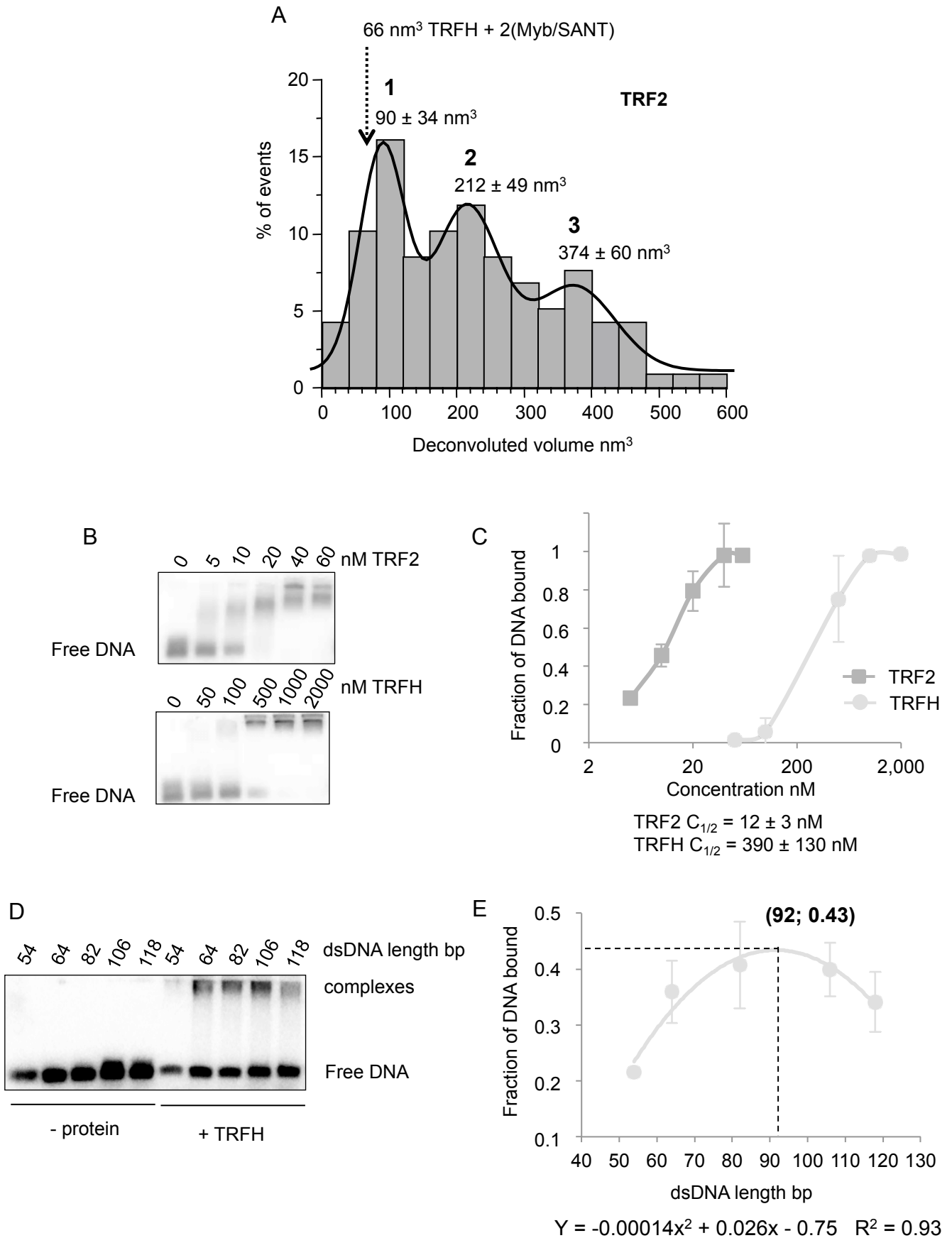
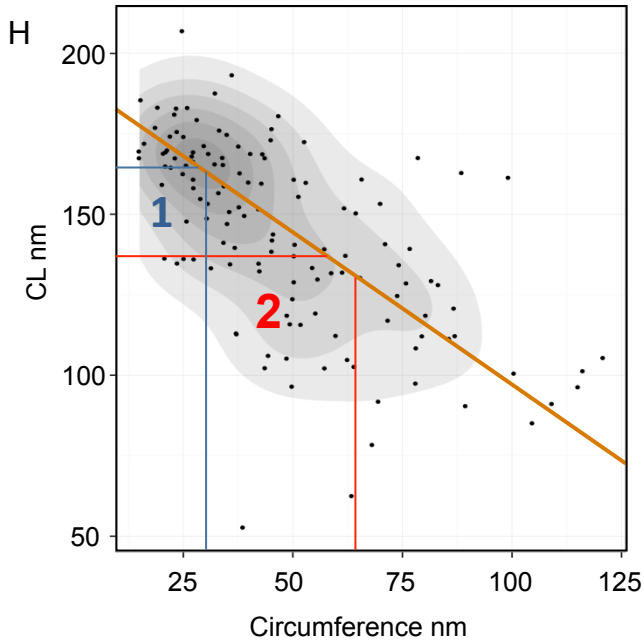
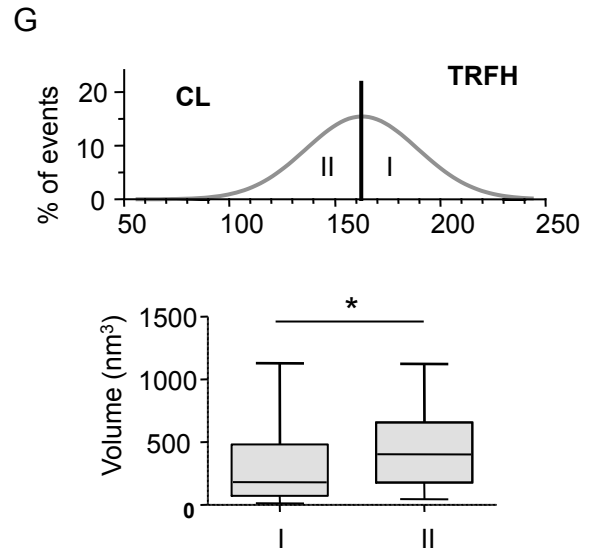
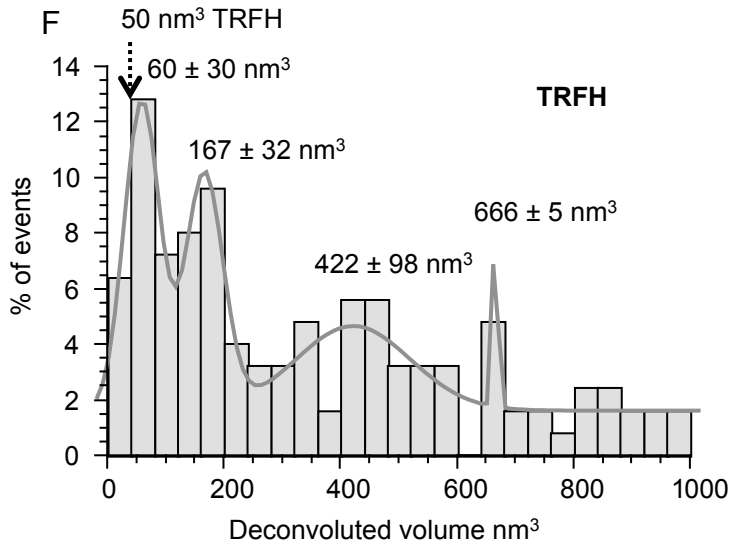


Figure S1



— Linear fit $y = -0.96x + 192$
 $R^2 = 0.35$

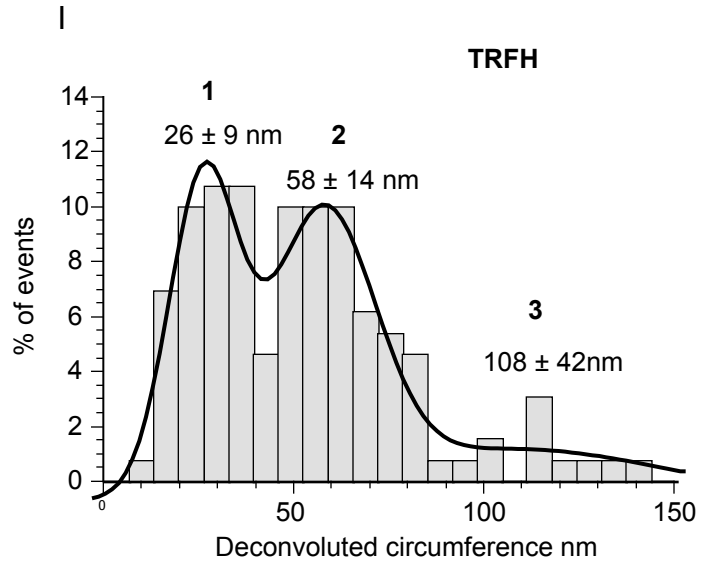
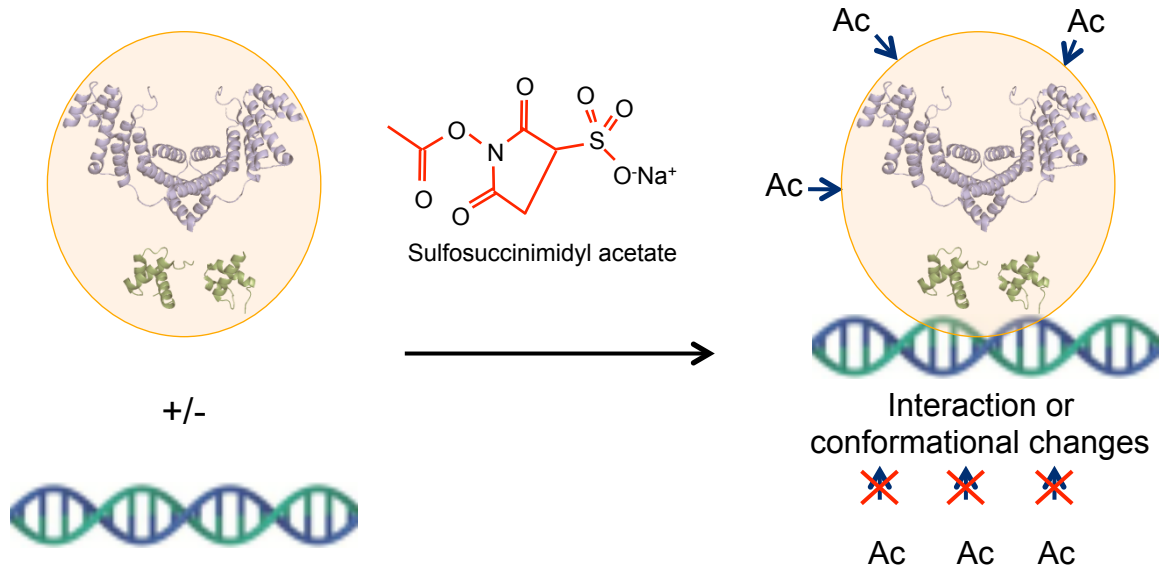
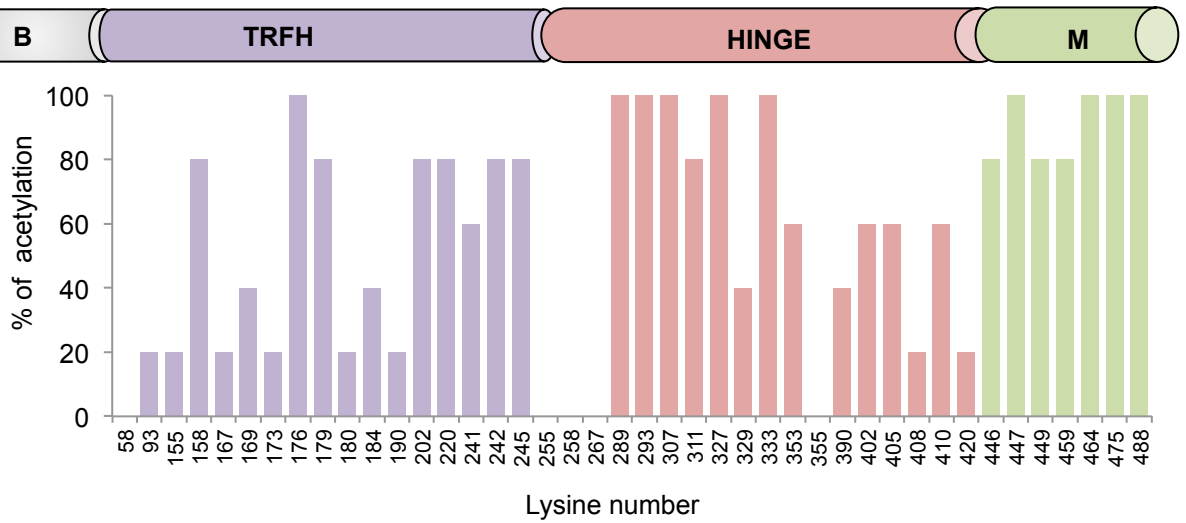


Figure S2

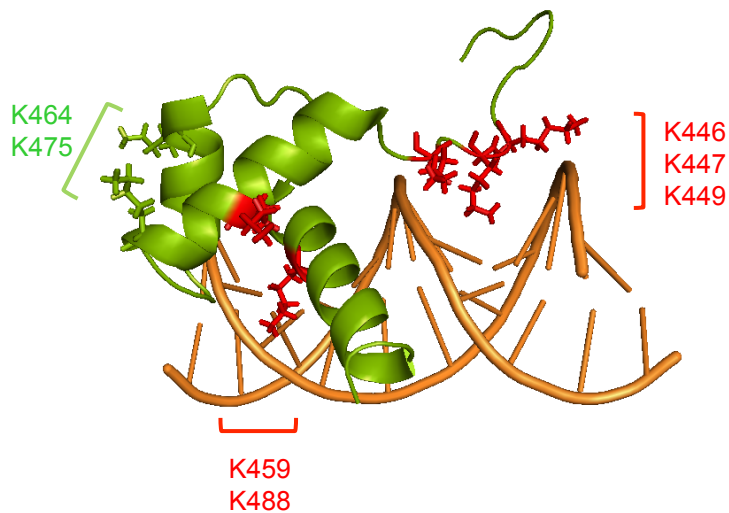
A



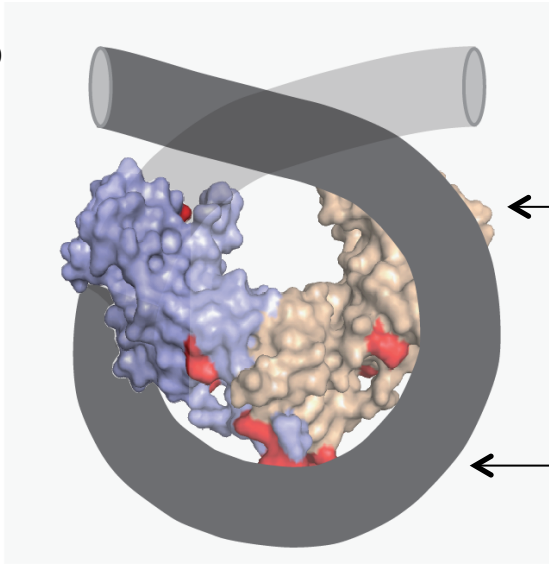
B



C



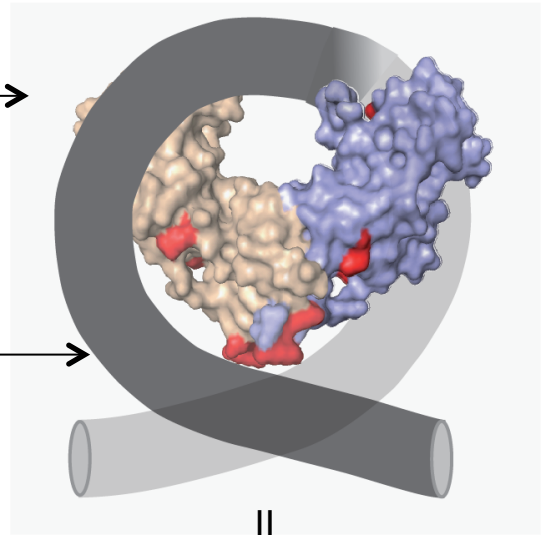
D



I
Right handed wrapping ✓

Top →

← Bottom



II
Left handed wrapping ✗

Figure S3

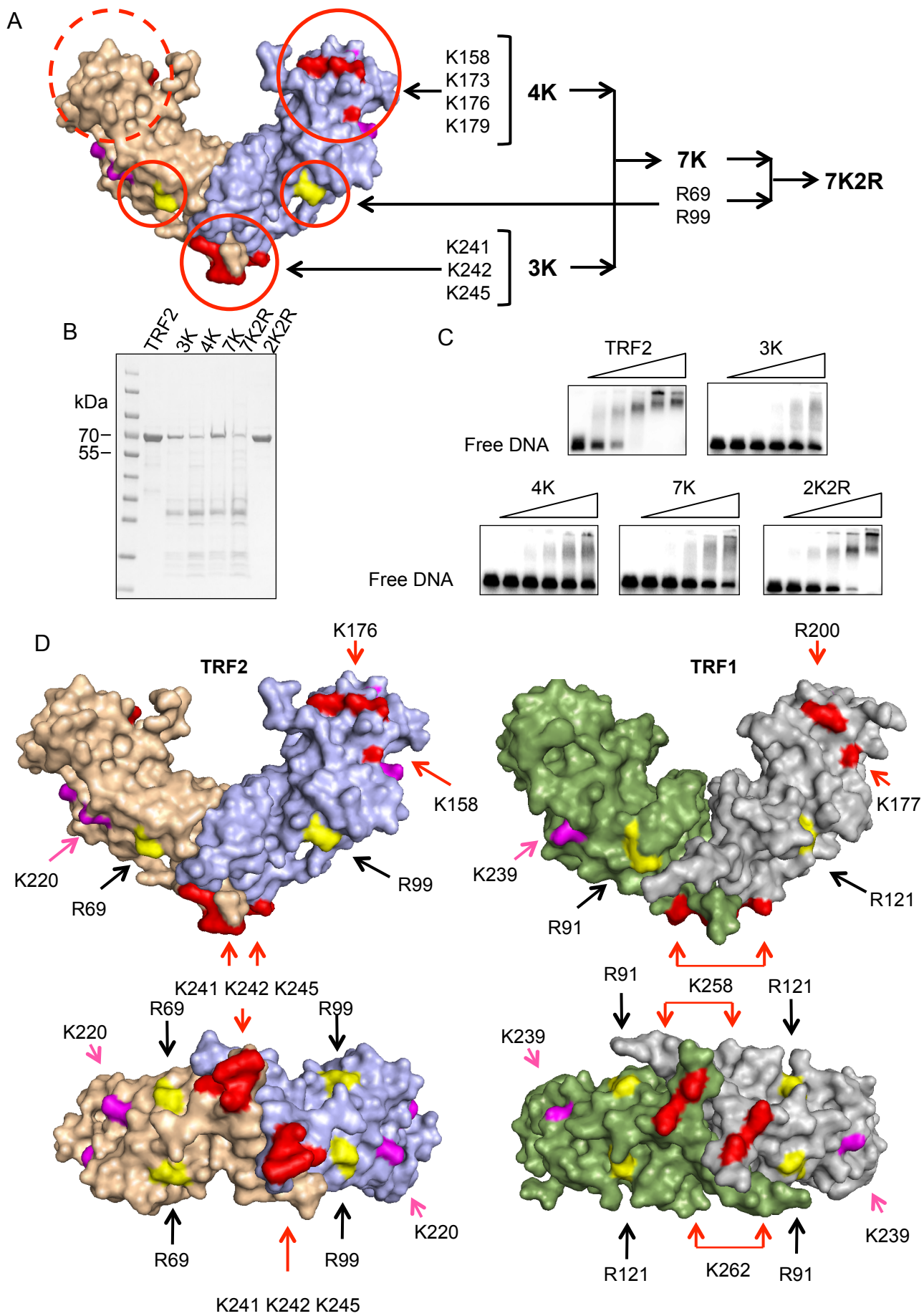


Figure S3

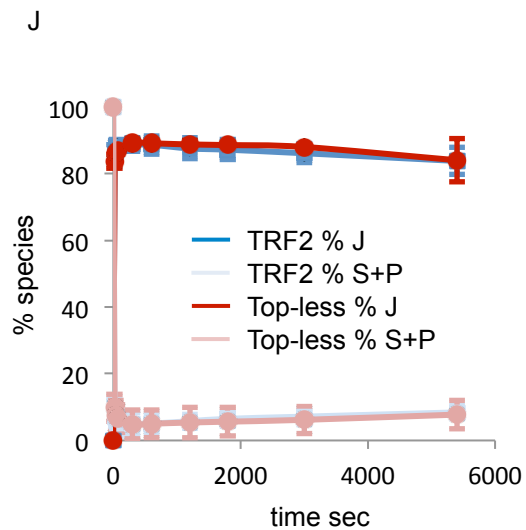
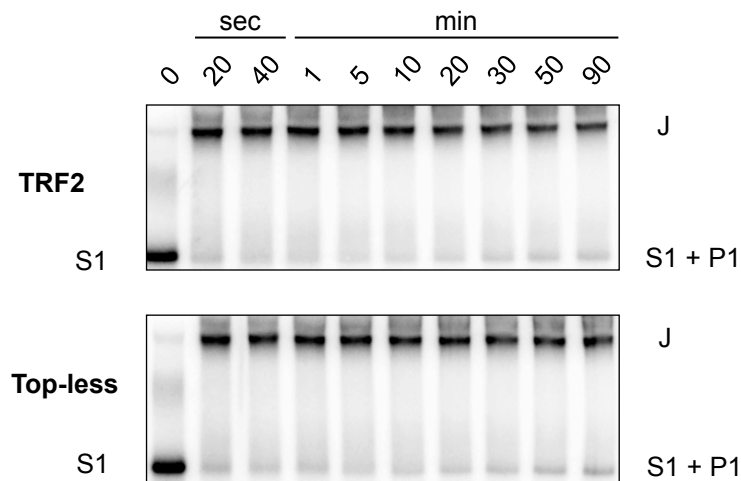
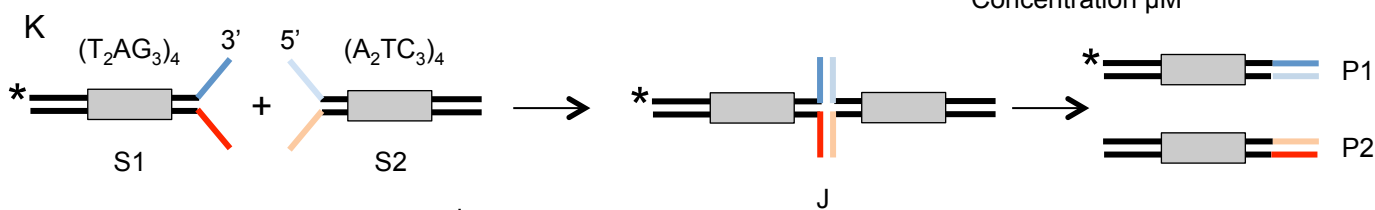
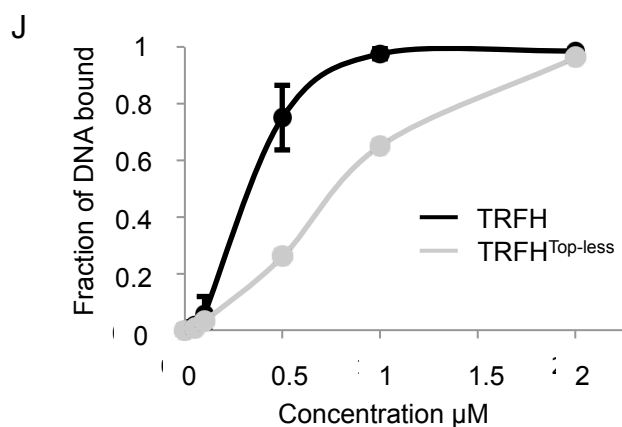
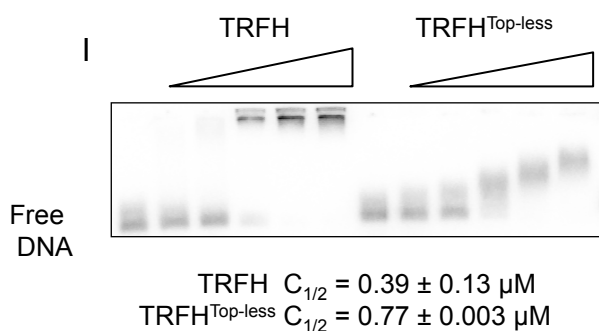
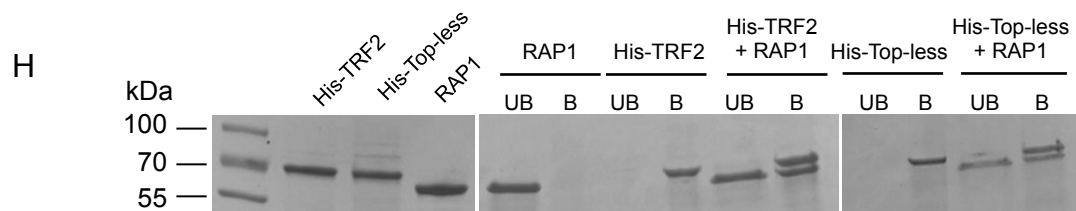
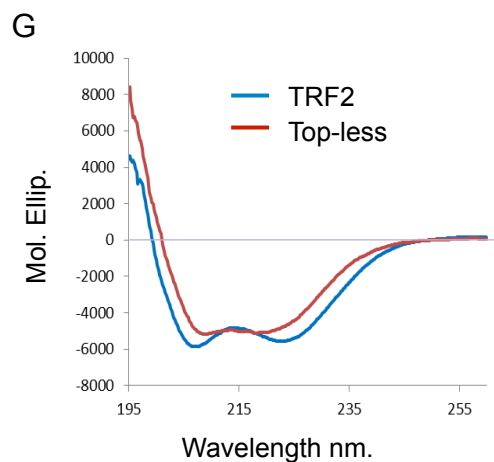
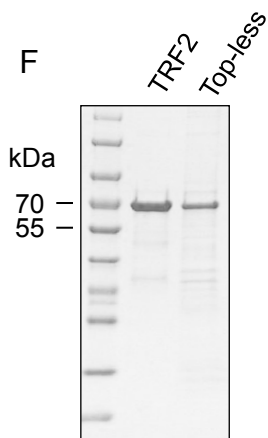
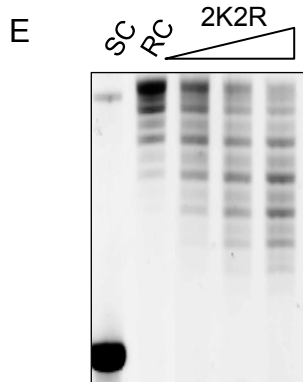
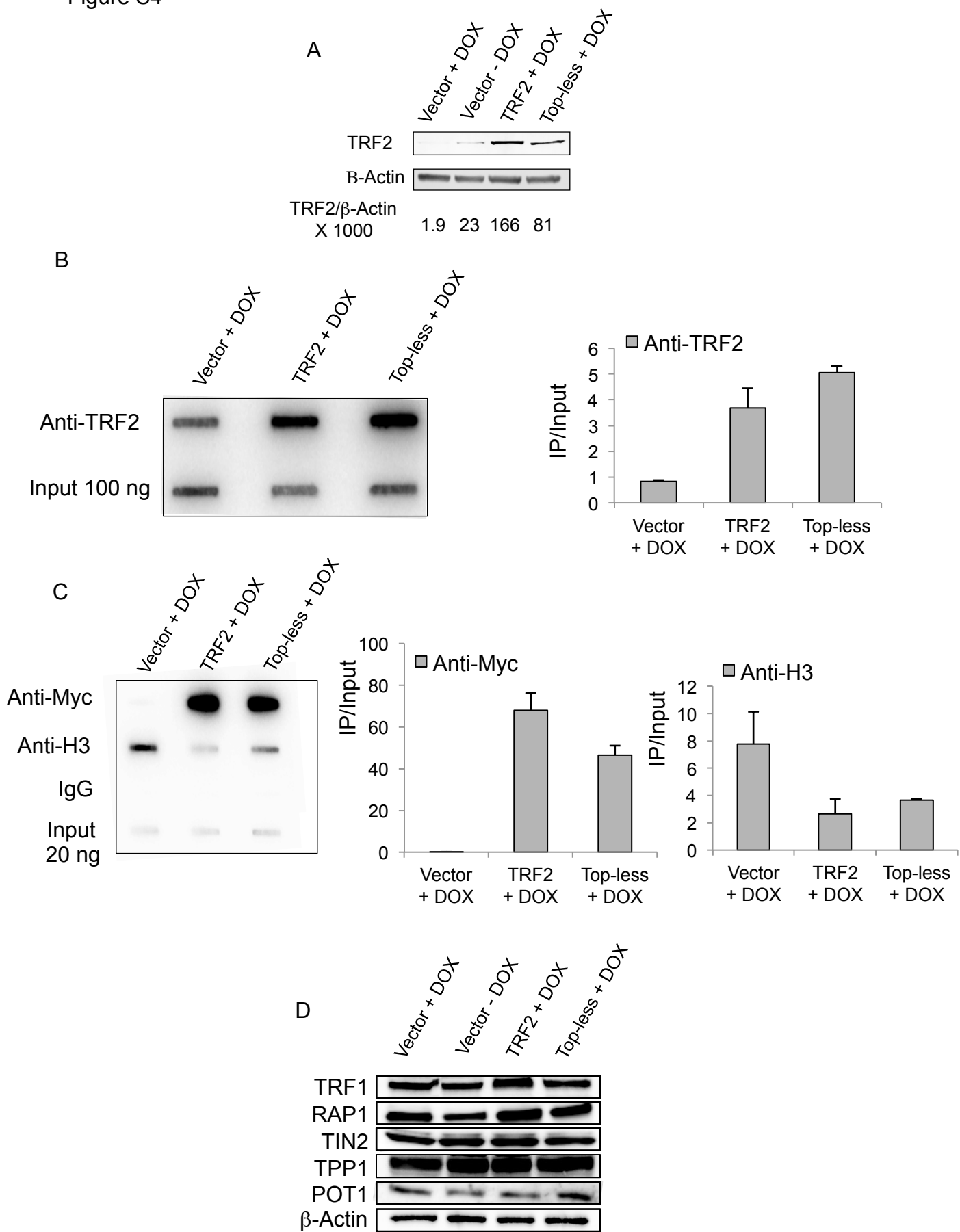
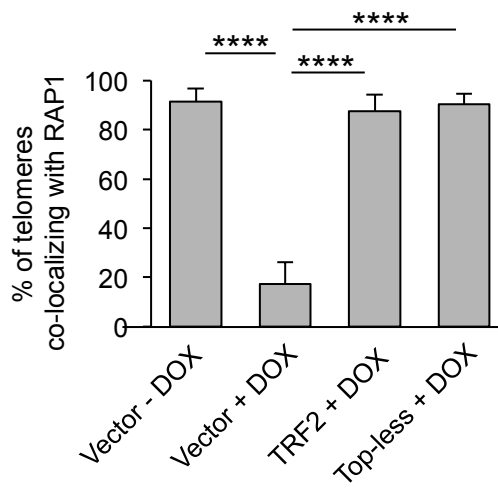
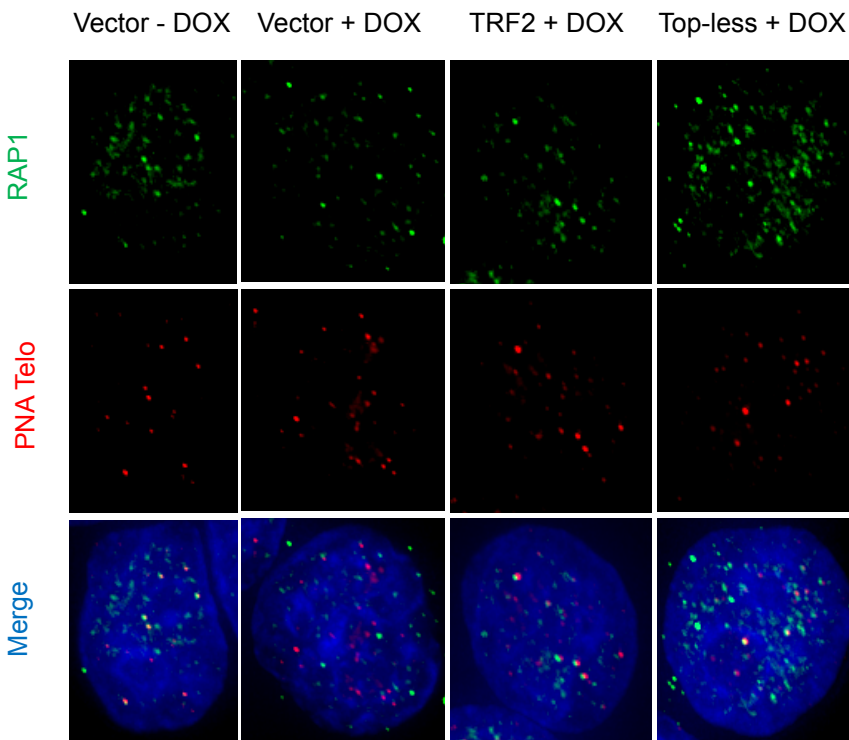


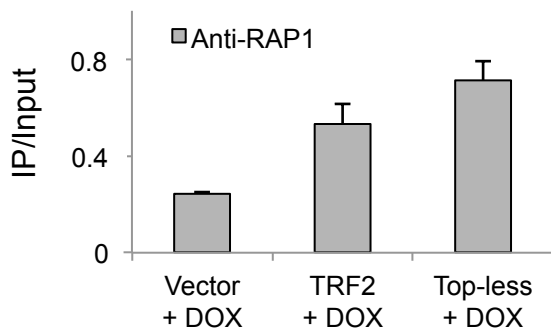
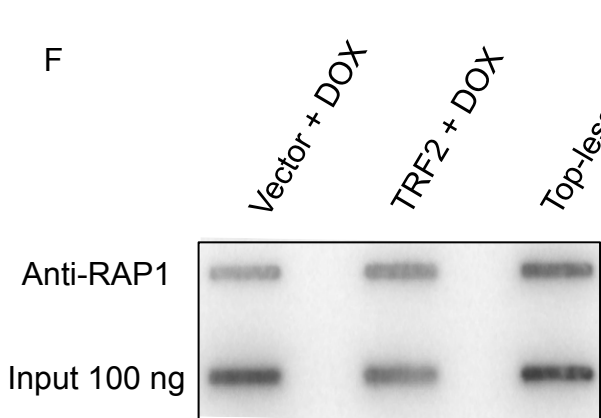
Figure S4



E Figure S4



F



G

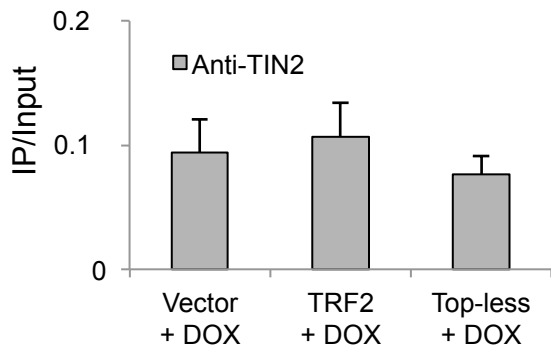
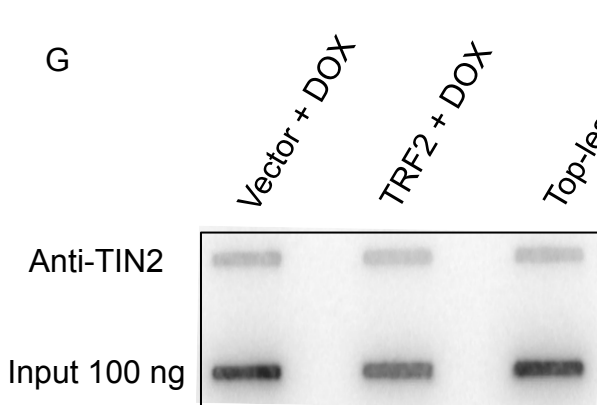


Figure S5

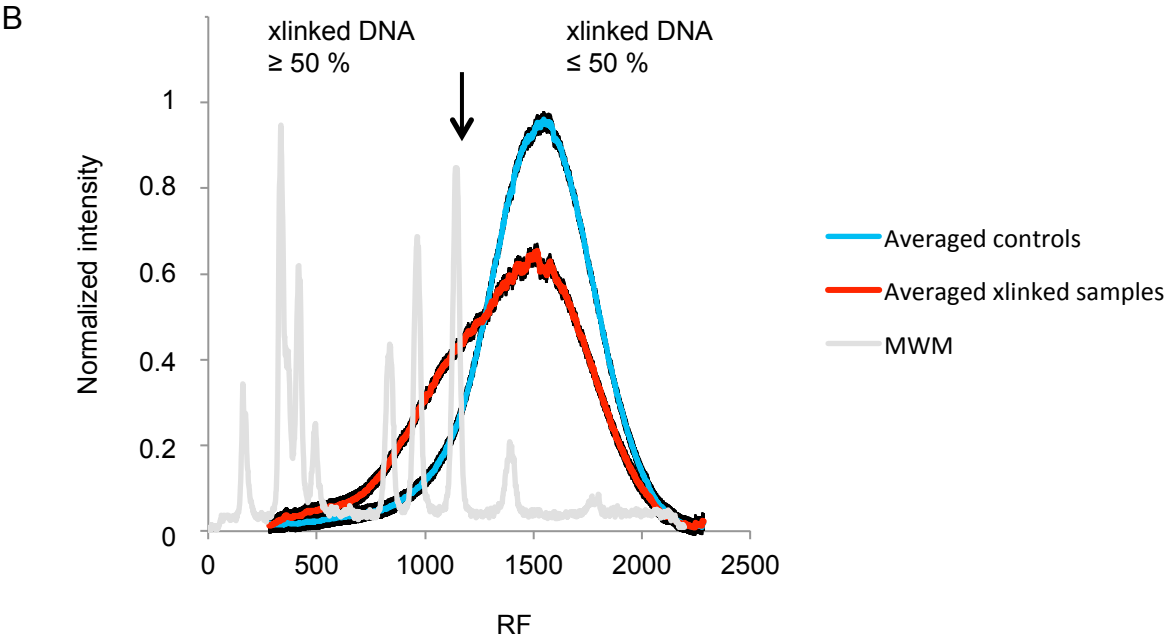
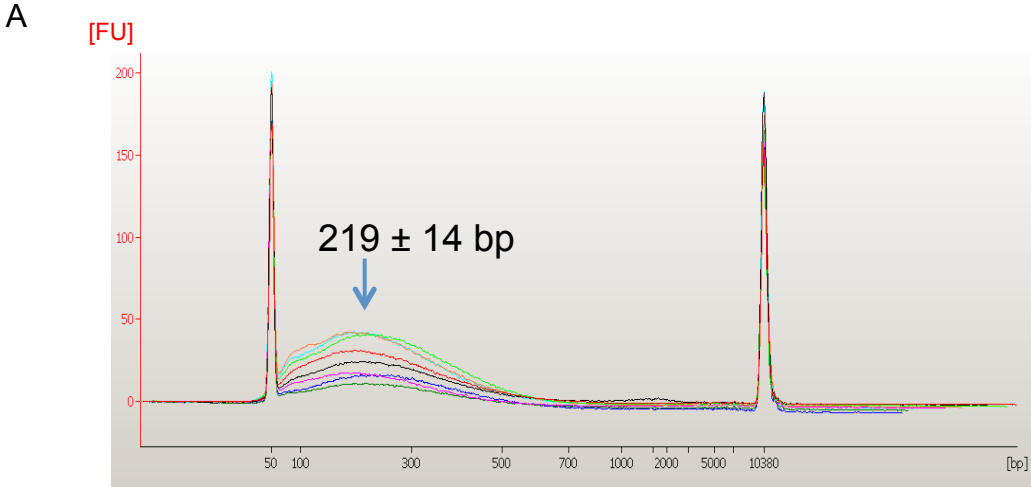
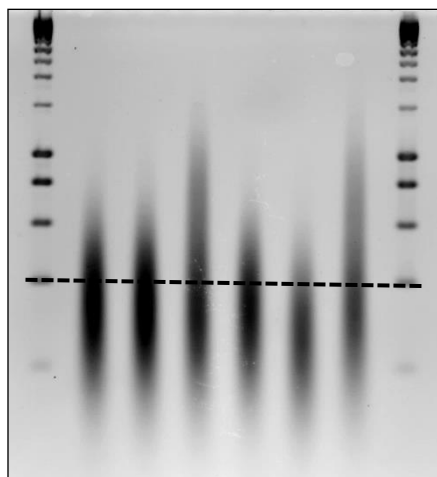


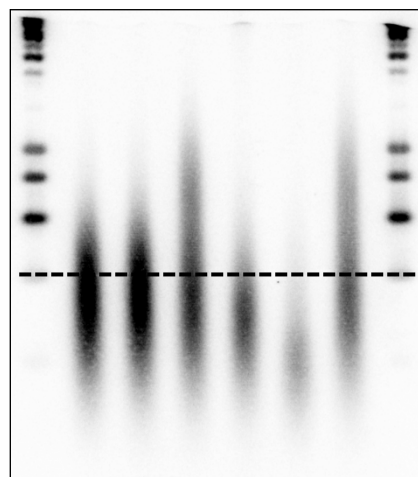
Figure S5

C Trioxsalen - + + - + +
 UV + - + + - +
 ICRF-193 - - - + + +



M M

D Trioxsalen - + + - + +
 UV + - + + - +
 ICRF-193 - - - + + +



M M

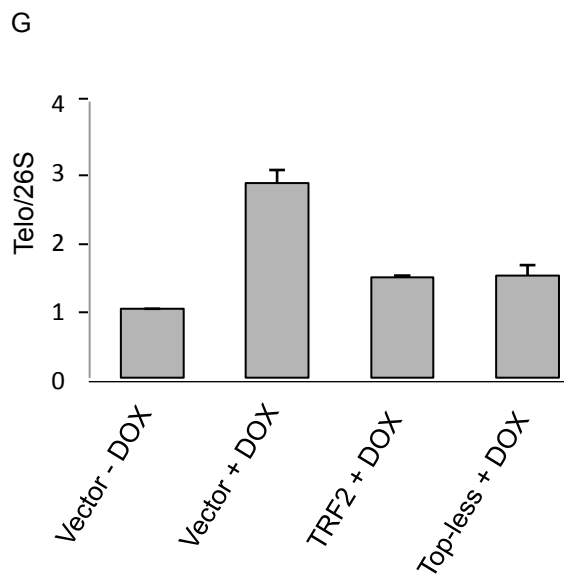
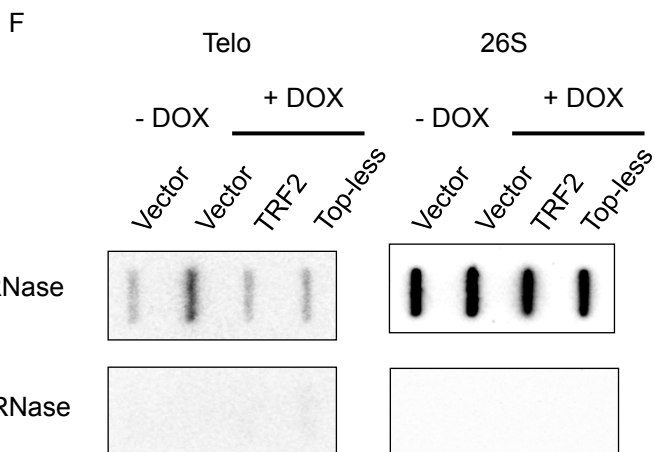
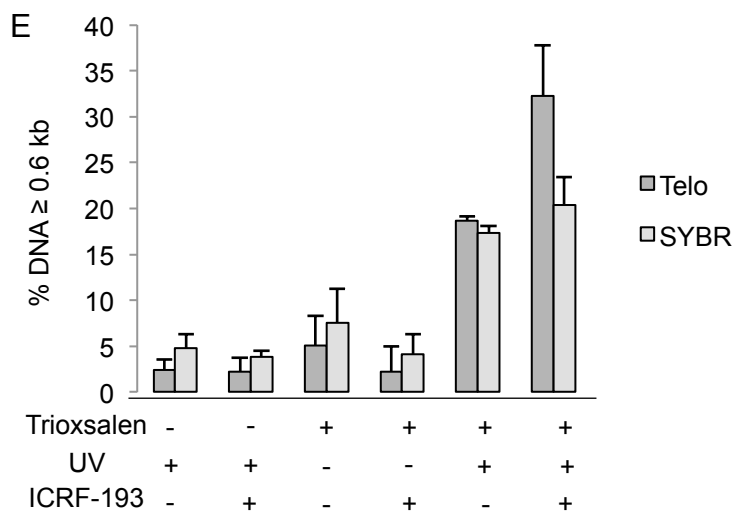


Figure S6

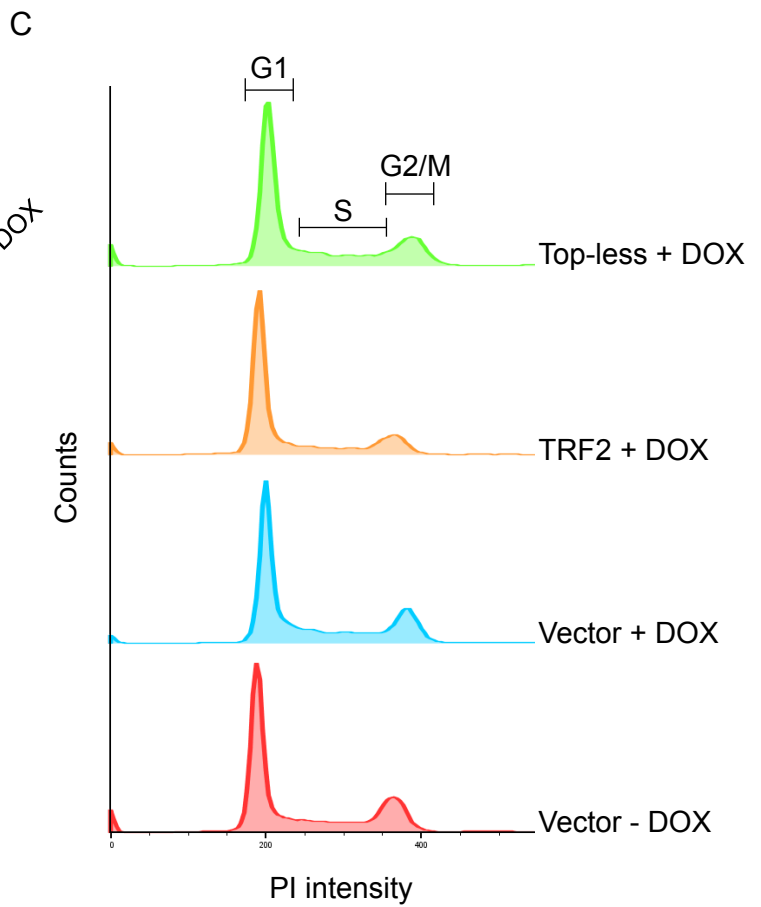
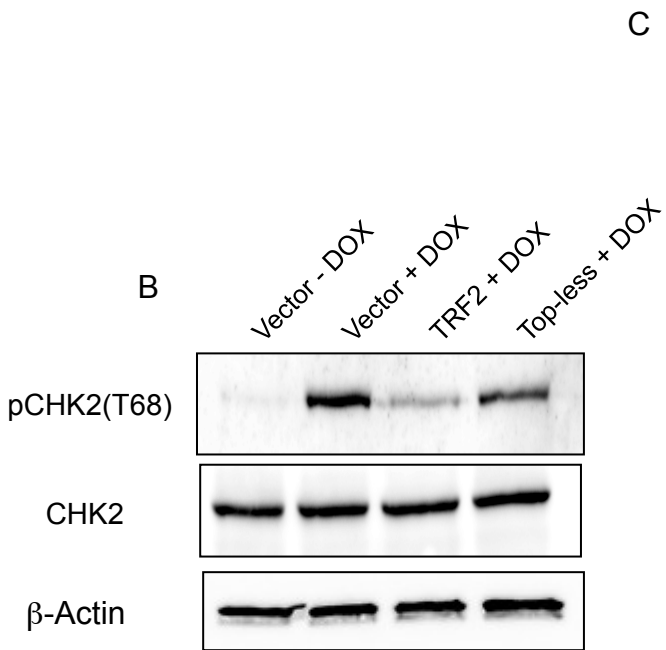
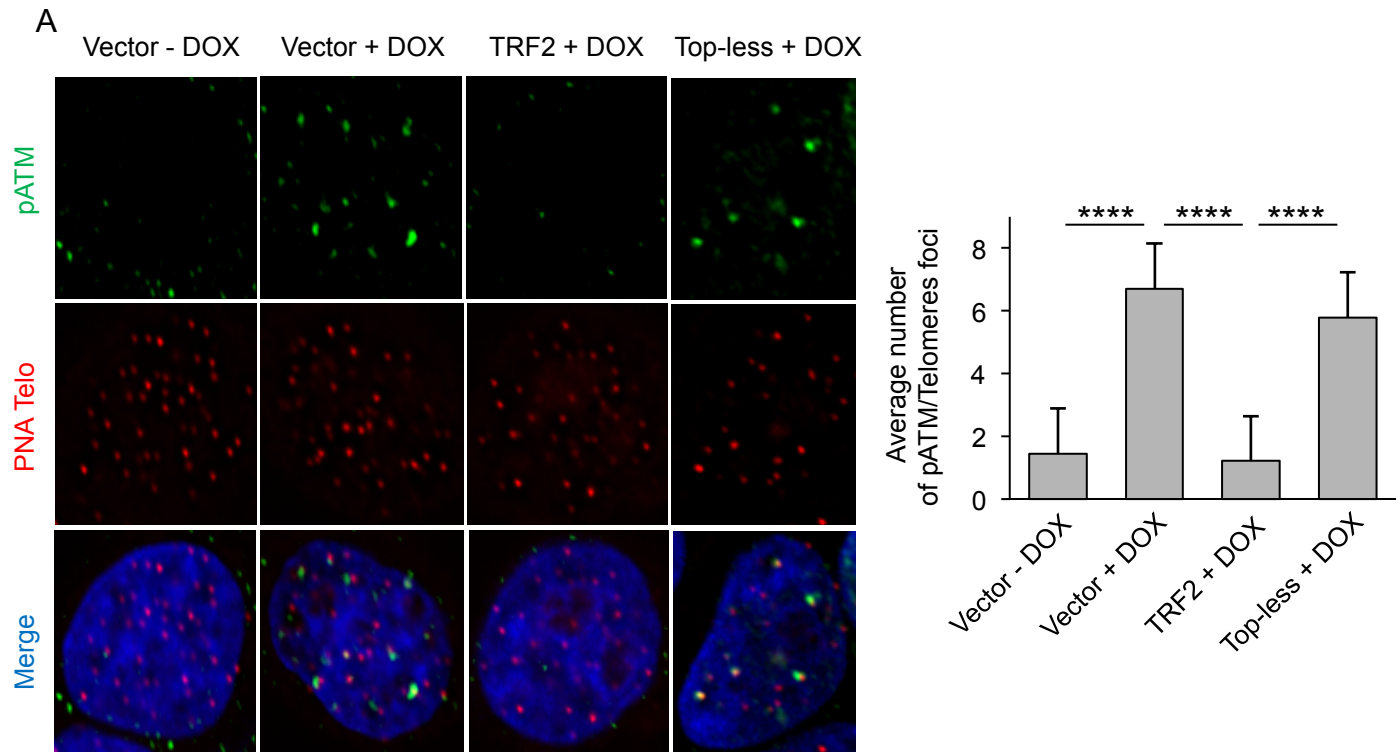
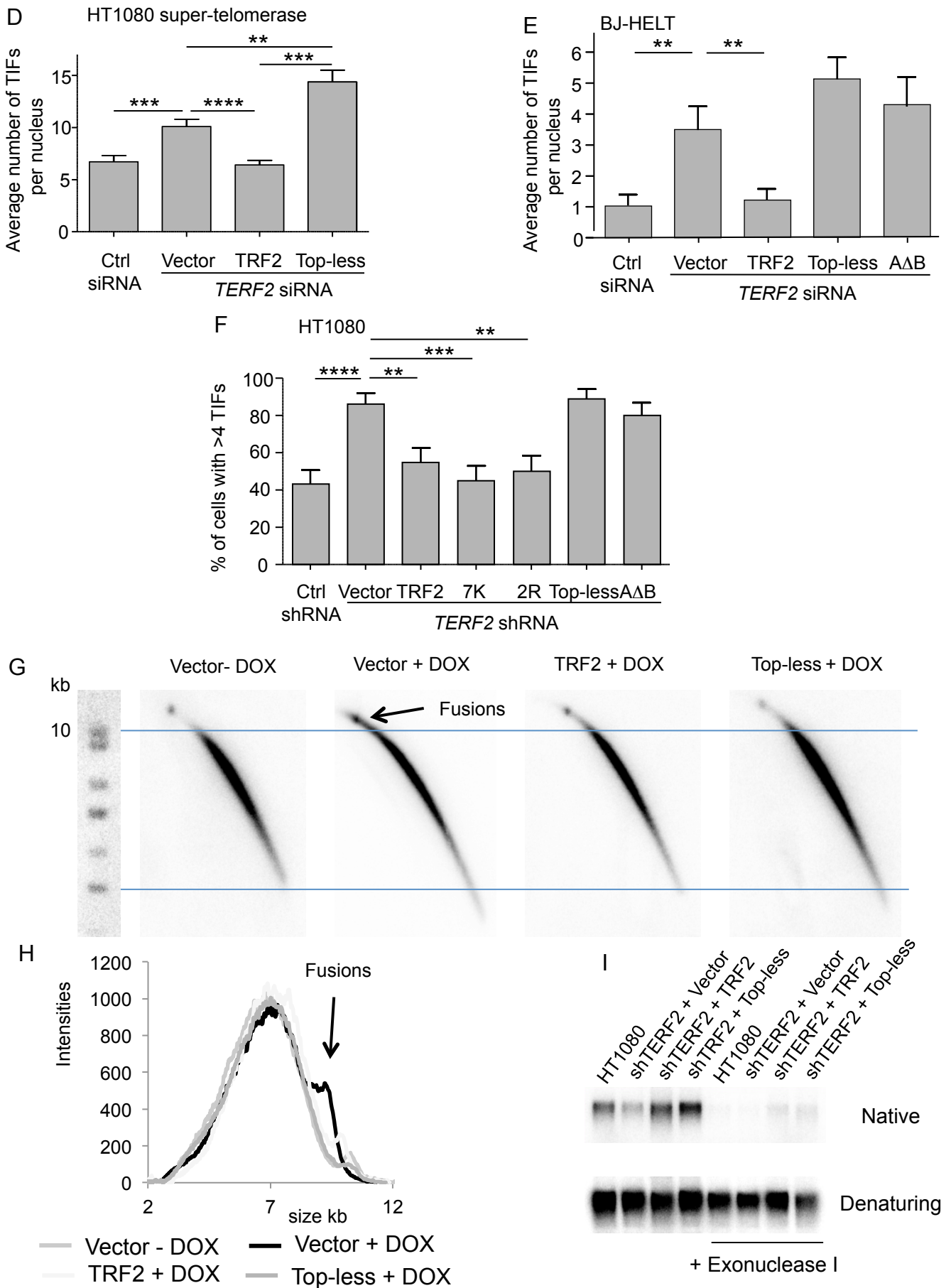


Figure S6



Supplementary Information

Supplementary figures legends

Figure S1. Volume and circumference distributions of DNA complexes in AFM experiments and DNA binding properties of the TRFH domain. Related to Figure 1.

(A) Distribution of deconvoluted volumes corresponding to the same set of TRF2/DNA complexes shown in Figure 1A. Histograms, expressed as percentage of events and corresponding to the raw data, were fitted with individual populations applying a Gaussian multi-peak fitting. The solid line corresponds to the sum of the multi-fitting. Note that the volume corresponding to the mean value of the first peak is bigger than the calculate volume of the TRFH + 2 Myb domains calculated from the 3D X-ray crystallography data (pdb 3BUA and 1VFC respectively) using the CRY SOL software. Peak 1 is thus compatible with the volume of a dimer.

(B) EMSA using labeled dsTelo106 as DNA probe and either TRF2 or TRFH.

(C) Quantitative analysis of EMSAs. Error bars represent standard deviations from three experiments.

(D) EMSA showing the binding of the TRFH domain at 250 nM on double stranded DNA probes of different lengths (54, 64, 82, 106, 118 bp) and containing 44, 54, 72, 96 and 108 bp of TTAGGG repeats respectively.

(E) Quantitative analysis of EMSAs. Error bars represent standard deviations from three experiments.

(F) Distribution of deconvoluted volumes for TRFH/DNA complexes calculated from AFM data shown in Figure 1B. Histograms correspond to raw data and curves to the sum of a Gaussian multi-peak fitting. Note that the value corresponding to the main volume of the first peak is very close to the volume of the TRFH domain calculated from the 3D X-ray cristallography data (pdb

3BUA) using the CRY SOL software. Peak 1 therefore corresponds to the binding of one dimeric TRFH domain.

(G) Top: Gaussian curve fitting the raw data for the CL distribution of TRFH/DNA complexes shown in Figure 1B. The distribution has been divided in two groups depending on their CL (CL > 163 nm and CL < 163 nm, group I and II respectively). Bottom: The volume distributions corresponding to the two CL groups were analyzed and represented in a box and whiskers graph. A p value < 0.05 was calculated for the difference between the medians of the 2 volume distributions, attesting that, as for TRF2, bigger complexes have smaller CL and *vice-versa*.

(H) 2D-probability density map of contour length (CL) and circumference obtained for the TRF2/DNA complexes representing the probability to find a protein/DNA complex with a given DNA contour length and the corresponding circumference. Note the slope close to 1 of the linear fit.

(I) Distribution of the calculated circumference for TRFH/DNA complexes obtained from the deconvoluted AFM data set shown in Figure 1B.

Figure S2. The acetylation footprinting method: principle and validation. Related to Figure 2.

(A) Schematics of the acetylation protocol. Purified TRF2 is acetylated *in vitro* by sulfosuccinimidyl acetate in the presence or absence of telomeric DNA. This compound only acetylates lysines accessible to solvent. Lysines protected either by DNA or through structural modifications caused by DNA cannot be acetylated. Mass spectrometry analysis gives acetylation profiles of the protein and thus allows the determination of protected lysines on the surface of the protein.

(B) Probability of acetylation (in %) for lysines in TRF2 reflecting their accessibility to solvent. Lysines 140 and 495 are not in the graph since their corresponding peptide were missing in the mass spectrometry profiles.

(C) NMR 3D structure (“PDB: 1VFC”) of TRF2 Myb/SANT domain bound to DNA. Lysines in red are located close to DNA, lysines in green are farther away. Note the nice correlation between proximity of DNA and protection shown in Figure 2.

(D) Positions of the protected lysines in the TRFH domain infer chirality in the interaction, thus forcing strands to cross. From earlier work (Amiard et al., 2007) we know that TRF2 introduces positive supercoils in a relaxed circular substrate. Two models can be drawn:

In I, DNA strands are crossing at the top of the TRFH structure giving a right handed wrapping. This would explain the positive supercoils caused by TRF2 in DNA.

In II, DNA strands are crossing at the bottom of the TRFH structure. In this case the wrapping is left handed. This does not fit with the positive supercoils reported.

Figure S3. Top-less: a mutant allowing separation between topology-related and unrelated functions of TRF2. Related to Figure 3.

(A) Positions of lysines and arginines mutated to alanine in the TRFH domain of TRF2. The dotted circle signals residues located at the back of the structure.

(B) Coomassie stained SDS-PAGE of mutants used in the activity (Topoisomerase I assay and EMSA) screening.

(C) EMSAs using the wild type and mutated proteins and the dsTelo106 probe. Protein concentrations were 5, 10, 20, 40 and 60 nM.

(D) Positions of mutated lysines and arginines in the TRFH domain of TRF2 and their corresponding residues in the TRFH of TRF1. Left: positions in TRF2 of lysines giving strong

signals in the footprint assay (red and pink) and of TRF1-conserved arginines (yellow); Right: TRF2-conserved lysines in TRF1 with the same color code than their corresponding residues in TRF2.

(E) Topoisomerase I assay for 2K2R. Protein concentrations used were 100, 250, 500 nM. Several non-relevant lanes were removed from the image. SC stands for supercoiled and RC relaxed circular DNA.

(F) Coomassie stained SDS-PAGE of purified TRF2 and Top-less proteins.

(G) Circular dichroism experiment performed with TRF2 and Top-less proteins.

(H) Coomassie stained SDS-PAGE showing recombinant His-tagged TRF2, His-tagged Top-less and untagged RAP1 proteins purified in *E. coli*. Recombinant RAP1 (15 μ g) was pulled-down with 10 μ g of recombinant TRF2 or Top-less proteins bound on cobalt-based magnetic beads. Unbound (UB) and bound (B) fractions were analyzed. Note the similar profile between wild type and mutated proteins showing a similar behavior for RAP1 *in vitro* binding.

(I) EMSA showing the binding of TRFH and TRFH^{Top-less} on dsTelo106. Protein concentrations used were 50, 100, 500, 1000 and 2000 nM. We noticed a qualitative difference in the nature of the complexes between both TRFH complexes. The wild type domain yielded complexes that did not run in 1% agarose, probably due to extensive distortion of DNA, while the mutated domain yielded complexes that resembled progressive binding of several proteins on less distorted DNA.

(J) Quantitative analysis of EMSAs. Error bars correspond to standard errors between three experiments.

(K) Formation and migration of a telomeric Holliday junction. Top panel: Schematics of the reaction. Two substrates (S1 and S2, S1 is ³²P labeled on the top strand) containing four human telomeric repeats and S1 to S2 compatible flapping ends were mixed together in the presence or absence of TRF2 or Top-less. Aliquots of the reaction were taken at different time points and the

nature of the species studied by migration in an acrylamide gel. One can observe the appearance of the slowly migrating four stranded Holliday junction (J). Since substrate (S) and product (P) were undistinguishable, quantification was done on the sum of the two species. Left panel: acrylamide electrophoretic analysis of aliquots at different time point. Right panel: quantitative analysis of the % of Holliday junction (% J) and % of the other species (% S+P) through time. Error bars correspond to standard deviation between three experiments. Note the identical behavior for both proteins.

Figure S4. Top-less binds telomeres in HeLa cells, does not modify shelterins expression and recruits RAP1 and TIN2 to telomeres as well as the wild type protein. Related to Figure 3.

(A) Immuno-blot using an anti-TRF2 antibody showing the expression of wild type or mutant TRF2 in HeLa cells treated or not with doxycycline (DOX) to induce TRF2 knock-down and transduced either with empty vector, TRF2 or Top-less expressing lentiviruses. Numbers below represent quantification of the membrane using the signal from β -Actin for normalization.

(B) ChIP experiment performed on TRF2 knocked down HeLa cells and transduced with viruses either containing an empty vector or expressing TRF2 or Top-less. ChIP was performed using an anti-TRF2 antibody. Membranes were hybridized using a telomeric probe (Telo). Quantification performed on two replicates is shown next. Error bars represent standard deviation.

(C) Same experiment as above using either an anti-Myc antibody, an anti-H3 antibody or an isotype IgG.

(D) Immuno-blots showing the expression of all other shelterin subunits in HeLa cells treated or not by doxycycline (DOX) to induce TRF2 knock-down and transduced either with empty vector, TRF2 or Top-less expressing lentiviruses.

(E) Co-localization of RAP1 (in green) with telomeres (in red) by PNA-FISH IF in the same cells as above. Nuclei were stained with DAPI. Quantification of the percentage of telomeres co-localizing with a RAP1 signal is shown below. Data represent the means \pm SE. P values were calculated using the Mann-Whitney test (**** P < 0.0001 and an absence of mark indicates no significance).

(F) ChIP experiment performed on TRF2 knocked down HeLa cells and transduced with viruses either containing an empty vector or expressing TRF2 or Top-less. ChIP was performed using an anti-RAP1 antibody. Membranes were hybridized using a telomeric probe (Telo). Quantification performed on two replicates is shown next. Error bars represent standard deviation.

(G) Same experiment as above using an anti-TIN2 antibody.

Figure S5. TRF2 controls telomeric DNA topology. Related to Figure 4.

(A) Bioanalyzer migration profiles of samples. A representative example is shown corresponding to the gel shown in Figure 4. An average size of 219 ± 14 bp was measured.

(B) Normalized profiles from all Southern blots of crosslinked (xlinked samples) DNA or non-crosslinked DNA (controls). Data from all experiments were averaged and plotted with the profile of Molecular Weight Markers (MWM). At the position corresponding to 0.6 kb the quantity of crosslinked and non-crosslinked material were equal in the crosslinked samples. Thus above this threshold DNA will be mainly crosslinked and below mainly un-crosslinked.

(C) Trioxsalen experiment performed with ICRF-193 treated cells. SYBRII stained glyoxal gel. M stands for molecular weight markers and the dotted line marks the 0.6 kb threshold used for analysis.

(D) Southern blot of the glyoxal gel hybridized by a telomeric probe (Telo).

(E) Quantitative analysis of glyoxal gels. The relative amount of DNA material above the 0.6 kb threshold was measured for each condition. SYBR indicates the values obtained for the SYBRII stained gels and Telo for the Southern blots. Error bars represent standard deviation from 4 experiments.

(F) Northern slot blot showing the amount of TERRA RNA in HeLa cells compromised for TRF2 (+ DOX) and transduced with viruses expressing either TRF2 or Top-less. The membrane was hybridized using either the 4C3 telomeric DNA probe (Telo) or a 26S probe (Vincent et al., 1993).

(G) Quantitative analysis of two northern slot blot experiments. The ratio between Telo and 26S signals was calculated for each slot in two experiments. Error bars represent min and max values of 2 replicates.

Figure S6. DDR activation in Top-less expressing cells. Related to Figure 5.

(A) Recruitment of the phosphorylated form of ATM (pATM) on Top-less telomeres. Co-localization of pATM (in green) with telomeres (in red) was analyzed by PNA-FISH and IF in HeLa cells treated or not with doxycycline (DOX) to induce TRF2 knock-down and transduced either with empty vector, TRF2 or Top-less expressing lentiviruses. Quantification of the number of foci colocalizing pATM and telomeres is shown next. Data represent the means \pm SE. P values were calculated using the Mann-Whitney test (**** P < 0.0001).

(B) Immuno-blots showing the presence of T68 phosphorylated CHK2 in HeLa cells knocked-down for TRF2 (+ DOX) and expressing the Top-less mutant compared to control or wild-type TRF2 expressing cells.

(C) Cell cycle analysis performed on the cells above using propidium iodine staining and analysis by Flow Cytometry.

(D) Co-localization of 53BP1 IF with a PNA-Telomeric probe revealing telomere dysfunction-induced foci (TIFs) in HT1080 super-telomerase cells transduced as indicated. Data show the mean \pm SE and P values were calculated using the Mann-Whitney test (** P < 0.01, *** P < 0.001, **** P < 0.0001). The quantification of *TERF2* transcript level for the different conditions of TRF2 expression (control siRNA with expression of empty vector, *TERF2* siRNA with expression of either empty vector or TRF2 or Top-less) was done by RT-qPCR and is respectively of 1.1, 0.2, 9.5, 6.5 fold of enrichment. These cells were used to measure the number of t-loops by STORM.

(E) Recruitment of 53BP1 on telomeres (TIFs) of BJ fibroblasts down-regulated for *TERF2* by siRNA and expressing either TRF2, Top-less or the A Δ B protein. Data show the mean \pm SE and P values were calculated using the Mann-Whitney test (** P < 0.01 and an absence of mark indicates no significance). The quantification of *TERF2* transcript level for the different conditions of TRF2 expression (control scramble siRNA with expression of empty vector, *TERF2* siRNA with expression of either empty vector or TRF2 or Top-less or A Δ B) was done by RT-qPCR and is respectively of 1, 0.13, 0.90, 0.79 and 0.97 fold of enrichment.

(F) Recruitment of 53BP1 on telomeres (TIFs) of HT1080 cells down-regulated for *TERF2* by shRNA and expressing either TRF2, and the 7K, 2R, Top-less and A Δ B mutants. Data show the mean \pm SE and P values were calculated using the Mann-Whitney test (** P < 0.01, *** P <

0.001, **** P < 0.0001 and an absence of mark indicates no significance). The quantification of *TERF2* transcript level for the different conditions of TRF2 expression (control scramble shRNA with expression of empty vector, *TERF2* shRNA with expression of either empty vector or TRF2 or 7K or 2R or Top-less or AΔB) was done by RT-qPCR and is respectively and 1, 0.7, 55, 65, 106, 16 and 68 fold of enrichment.

(G) 2D gels of genomic DNA from HeLa cells compromised for TRF2 (+ DOX) and infected with viruses expressing either the empty vector, TRF2 or Top-less. The horizontal lines mark the 10 kb and 3 kb sizes. Note the presence of slowly migrating species for the Vector + DOX sample indicating the presence of fusions.

(H) Migration profiles were obtained for each 2D gel and the corresponding intensities reported as a function of the sizes thanks to size markers run beside each sample. Note the shoulder on the Vector + DOX curve corresponding to the fusions.

(I) In-gel 3' overhang experiment, performed with and without Exonuclease I treatment, showing the amount of telomeric single strand overhang (Native) and total telomeric DNA (Denaturing) in HT1080 cells compromised for TRF2 (sh*TERF2*) and transduced with viruses either containing an empty vector or expressing TRF2 or Top-less. Note the expected decrease in overhang due to the presence of the sh*TERF2* and the rescue by both the wild type and mutant proteins.

Material and Methods

AFM imaging

Complexes deposition:

10 μl of a solution of DNA and proteins in 5 mM HEPES pH 7.4, 150 mM KCl and 1 mM MgCl₂ was incubated 20 min at 25°C. The protein/DNA molar ratios used were the following: (2.5/10) nM for TRF2, (1100/7) nM for TRFH, (5/10) nM for Top-less. After incubation, samples

were crosslinked with glutaraldehyde (0.1% final concentration) for 30 min on ice. Before applying the sample on freshly cleaved mica, the concentration of MgCl₂ was increased to 10 mM. After 2 min on mica the sample was washed with 1 ml of deionized water and dried under a gentle N₂ flow. Imaging was performed on a Multimode 8 equipped with E-scanner controlled by a Nanoscope V (Bruker AXS, Santa. Barbara, CA), in air under Tapping Mode using silicon tips (RTESP, 300kHz). Images were recorded at 1.5–2.0 Hz over 1 μm wide scan area (512×512 pixels). Raw images were flattened using the manufacturer's software (Nanoscope Analysis 1.40) and converted into TIF files.

Contour Length and volume measurements:

Contour lengths (CLs) for each molecule were manually traced and measured using Image J software (<http://imagej.nih.gov/ij/>). For DNA-protein complexes the read-through DNA length method was used. Measurements of the naked DNA were performed using the naked molecules found in the images corresponding to the different binding experiments.

Although, the expected contour length for a B-DNA molecule of 650 bp is 221 nm (650 bp* 0.34 nm/bp), the measured mean values obtained for each naked DNA is shorter (192 ± 11 nm, 189 ± 9 nm and 188 ± 9 nm for TRF2, TRFH and Top-less binding experiment respectively). This discrepancy is related to a DNA shortening possibly due to a partial B- to A-form transition induced by the drying step (Rivetti and Codeluppi, 2001). The mean helical rise corresponding to the three different naked DNA mean CLs is then 0.29 nm/bp, that gives rise to 93 bp of DNA wrapping (27nm/0.29 nm/bp).

Volumes were calculated as ellipsoids using the formula:

$$V = \frac{4}{3} * \pi * (D/2 * d/2 * h)$$

where D, d and h correspond to major diameter, minor diameter and height respectively.

These parameters were measured using Image SXM software (www.liv.ac.uk/~sdb/ImageSXM). At least 130 objects were scored for each condition.

Volume deconvolution:

The dimensions of an object imaged by AFM are affected by the broadening effect due to the tip-sample convolution radius. The relationship between the experimental width of the sample in the image, W , the radius of curvature of the tip, R_c , and the radius of curvature of the sample, R_m , is given by the equation (Bustamante et al., 1993):

$$W = 4R_c R_m^{1/2}$$

If two objects are measured with the same probe the ratio between them is the following:

$$W_1/W_2 = (R_1/R_2)^{1/2}$$

The double-stranded DNA width (2 nm), involved in the protein complex, can be used as an internal reference for size. This allows us to obtain the real diameters for the protein complex (Nettikadan et al., 1996).

$$R_1 = (W_1/W_2)^2 * R_2$$

Where R_1 and R_2 are the real dimensions of the protein complex and the DNA respectively, while W_1 and W_2 are their measured dimensions.

Using the deconvoluted values corresponding to the protein diameters, it is possible to calculate the deconvoluted volumes.

Circumference estimation :

Once the deconvoluted values for the minor d and major D diameters are obtained, using the Ramanujan approximation it is possible to calculate the deconvoluted circumference of the ellipsoid using the following formula:

$$C \approx \pi * (3*(d+D) - ((3d+D)*(d+3D))^{1/2})$$

Plots and statistics :

All the histograms represent the distribution of a measured or calculated parameter expressed in percentage of events. To obtain the mean value corresponding to each subpopulation emerging from multimodal distributions, a multi-Gaussian fitting has been applied using the QtiPlot data analysis and scientific visualization (<http://soft.proindependent.com/qtiplot.html>). All the parameters obtained by the Gaussian fitting are expressed in the text as mean \pm FWHM (Full width at half maximum). The 2D-probability density map of contour length (CL) and circumference measured by AFM for the complexes TRF2/DNA is obtained using R open source software (<http://www.R-project.org>). The software was used to calculate the bivariate kernel density estimation. The resulting 2D map represents the probability to find a protein/DNA complex with a given DNA contour length and the corresponding protein circumference. The darker the region in which the data fall, the higher is their probability density.

The linear fit applied to the scatter plot corresponding to the correlation graph of CLs as a function of circumferences for TRF2/DNA complexes was performed imposing a y-intercept of 192 nm (mean value of the corresponding naked DNA) and calculated using the QtiPlot software. The analysis of the TRFH/DNA volume distributions as a function of TRFH/DNA CL distribution was performed using GraphPad Prism v 5.03. The results are shown as a box and whiskers plot. To the two volume populations the Wilcoxon matched-pairs signed rank test was applied giving a p value < 0.05 .

Strand invasion assay, topology assays, EMSAs, and Holliday junction migration assays

Strand invasion assays were performed as described previously (Poulet et al., 2012). Topology assays were also performed as described previously (Amiard et al., 2007; Poulet et al., 2012), but using pLTelo, a pLEU500-Tc (Chen et al., 1992) -based plasmid containing 650 bp of human telomeric repeats between *Bst*API and *Bam*HI sites. EMSAs were performed using a 106-bp DNA probe containing 16 TTAGGG repeats flanked by a 5-bp (CAGCC) sequence at the 5'

and a 5 bp (CCTTG) sequence at the 3' end. A total of 5 nM of 5' labeled probe was incubated in a total volume of 10 μ l in 20 mM HEPES pH 8, 100 mM NaCl, and 500 ng/ μ l of acetylated BSA on ice for 15 min. Ficoll was added to a final concentration of 3% and the samples loaded on a 1% agarose gel with 0.5 \times TBE under 7 V/cm. Migration was performed at the same voltage for 30 min. The gels were then dried and analyzed using phosphorimager screens. Analysis was performed on a Typhoon FLA 9500 (GE Healthcare) using the Image Quant software (GE Healthcare). Holliday junction migration assays were performed as described previously (Poulet et al., 2009).

Circular dichroism (CD)

Far-UV CD spectra (between 195 nm and 260 nm) were recorded using a Jasco J-815 spectropolarimeter equipped with a Peltier temperature control unit. The spectra were acquired as an average of five scans with a scan speed of 100 nm/min and a response time of 2 s. CD measurements were performed at 20°C, using 1-mm quartz cells. TRF2 and Top-less samples were at 4.6 μ M in 10 mM Tris buffer, pH 8.0, 60 mM NaCl, 10% glycerol, and 0.2 mM DTT.

Pull-down assay

A total of 10 μ g of purified His-fusion TRF2 or His-fusion Top-less proteins were incubated with cobalt-based magnetic beads (Dynabeads, Lifetechnologies) at 4°C for 30 min in 50 mM sodium phosphate pH 8, 300 mM NaCl, and 0.01% Tween 20. After two washes using the same buffer, 15 μ g of purified Rap1 were added at 4°C for 90 min. The supernatant (unbound fraction, UB) was precipitated with cold acetone and resuspended in Laemmli loading buffer. After two washes, the magnetic beads containing the His-tagged proteins and associated Rap1 protein (bound fraction, B) were resuspended in Laemmli loading buffer and analyzed by SDS-PAGE.

Direct Stochastic Optical Reconstruction Microscopy (STORM) experiments

Preparation of nuclei, psoralen crosslinking and chromatin spreading :

Samples were prepared using the protocol described in Doksani et al (Doksani et al., 2013) with minor modification: 5×10^6 nuclei (HT1080 super-telomerase cells with down-regulation of endogenous *TERF2* by siRNA and ectopic expression of TRF2 or Top-less) were isolated as described in Pipkin and Lichtenheld, 2006 (Pipkin and Lichtenheld, 2006), resuspended in 1 ml of NWB (10 mM Tris-HCl pH 7.4, 15 mM NaCl, 60 mM KCl, 5 mM EDTA, 300 mM sucrose), and incubated in a 3.5 cm dish, on ice, in the dark, while stirring for 5 min with 100 µg/ml Trioxsalen (SIGMA). Nuclei were exposed to 365 nm UV light at 2 cm from the light source (model UVL-56, UVP) for 30 min, while stirring on ice. After crosslinking, nuclei were collected, washed once with ice-cold NWB, and resuspended in 250 µl of NWB. For spreading, nuclei were diluted 1:10 in spreading buffer (10 mM Tris-HCl 7.4, 10 mM EDTA, 0.05% SDS, 1 M NaCl, pre-warmed at 37°C) and 100 µl of the suspension was immediately spread on a 18 mm diameter 1.5H coverslip (Marienfeld) using a Shandon Cytospin 3 (600 rpm, 1 min, medium acceleration). Samples were fixed in methanol at -20°C for 10 min followed by 1 min in acetone at -20°C. The coverslips were washed in PBS 1x and dehydrated through a 70%, 95%, 100% ethanol series before performing FISH.

Fluorescence in situ hybridization

The PNA probe [CCCTAA]₃, conjugated with Alexa Fluor 647 fluorophore (PNA Bio INC.), was resuspended in water at a stock concentration of 20 µM and diluted 1:100 in the hybridization buffer solution (70% formamide, 10 mM Tris-HCl pH 7.2, 1:10 blocking buffer) before FISH labeling. 10 µl of this solution was put on a glass slide and ethanol-dried samples on coverslips were then put on top of the drop. The slide-coverslip “sandwich” was placed at 80°C for 10 min on heat block, with the slide-side facing the block, to allow DNA denaturation.

Then the samples were put overnight in the dark at room temperature in a humidified box in order to let the hybridization reaction to occur. The coverslip was then removed from the slide and washed twice for 15 min with 70% formamide; 10 mM Tris-HCl pH 7.2 and 3 times for 5 min with 0.1 M Tris-HCl pH 7.2, 0.15 M NaCl, 0.08% Tween-20, at room temperature and finally with PBS 1x. YOYO-1 (1:20000 in PBS1x) was dropped on samples and immediately washed with PBS 1x. Coverslips were then covered with PBS1x and directly used for imaging.

dSTORM imaging and analysis

The stained coverslips were imaged the same day at room temperature in a closed chamber (Ludin Chamber, Life Imaging Services) mounted on an inverted motorized microscope (Nikon TI-E) equipped with a 100x 1.49 NA PL-APO objective and a Perfect Focus System (Nikon), allowing long acquisition in oblique illumination mode. Imaging was performed in an extracellular solution containing reducing agents and oxygen scavengers. For dSTORM, Alexa-647 was first converted into dark state using a 642 nm laser (Coherent) at 30–50 kw/cm² intensity. Once the ensemble fluorescence was converted into the desired density of single molecules per frame, the laser power was reduced to 7–15 kw/cm² and imaged continuously at 10 fps for 5,000 frames. The level of single molecules per frame was controlled by using a 405 nm laser (Omicron). The laser powers were adjusted to keep an optimal level of stochastically activated molecules during the acquisition. Single molecule fluorescence was collected by a TIRF-Quad filter set 405/488/561/640 (F66-04TN from AHF analysentechnik AG). The fluorescence was collected using a 512x512 EMCCD (Evolve, Photometrics). The acquisition and localization sequences were driven by MetaMorph 7.8.3 and Wavetracer 1.5 software (Molecular Devices) in streaming mode at 10 frames per second (100 ms exposure time) using the full chip of the camera. Single molecule localization and re-construction were performed offline using Wavetracer and GPU acceleration. The reconstructed images were analyzed by

Image-J software (Rasband, W.S., ImageJ, U. S. National Institutes of Health, Bethesda, Maryland, USA, <http://imagej.nih.gov/ij/>, 1997-2014) taking into account only the objects having a length $\geq 1500 \mu\text{m}$ (corresponding to 5000 bp). Molecules having gaps longer than $0.5 \mu\text{m}$ and kinked, knobbed-like or branched molecules were not scored as in Doksani et al. (Doksani et al., 2013).

Western blots

A total of $30 \mu\text{g}$ of total extract was loaded on a 4-20% acrylamide gradient SDS gel in Laemmli buffer. After separation, proteins were transferred on an Immobilon-FL PVDF membrane (Millipore) and TRF2 was revealed using an anti-TRF2 primary antibody from mouse (Imgenex IMG-124A) and an IRdye-labeled goat anti-mouse antibody (Li-Cor) under the conditions recommended by the supplier. Bands were revealed using the Odyssey apparatus and corresponding software (Li-Cor). For shelterin proteins, the following antibodies were used: Rabbit Polyclonal anti-TRF1 (Santa Cruz Biotechnology, Inc., sc-6165-R); Rabbit Polyclonal anti-POT1 (Novus Biologicals, NB100-56429); Rabbit Polyclonal anti-TPP1 (Bethyl Laboratories, Inc., A303-069A); Rabbit Polyclonal anti-TIN2 (Abcam, ab64386); Rabbit Polyclonal anti-RAP1 (Bethyl Laboratories, Inc., A300-306A); Rabbit Monoclonal anti-CHK2 (phospho T68), Abcam ab32148; Mouse Monoclonal anti-CHK2 (BD Biosciences, 611571).

Chromatin immunoprecipitation

Anti-Myc ChIP was performed as described previously (Simonet et al., 2011) with minor modifications. Briefly, HeLa cells were cross-linked for 12 min with 1% formaldehyde and washed with cold PBS. Cells were centrifuged and the pellet was resuspended in cell lysis buffer (5 mM PIPES pH8, 85 mM KCl, 0.5% NP40 and protease inhibitors). The cells were disrupted with a dounce homogenizer and centrifuged at 4°C . The pellet was resuspended in nucleus lysis

buffer (50 mM Tris-HCL pH 8, 10 mM EDTA, 1% SDS, protease inhibitors) and cells were sonicated using a Bioruptor to obtain an average fragment size of 400 bp. IPs were set up with 40 µg of DNA, and Myc-Tag (9B11 Cell Signaling, mouse) and H3 (1791 abcam, rabbit polyclonal) antibodies were incubated overnight. Magnetic beads (Dynabeads, Life Technologies) were added for 2 hours. The beads were washed with a low salt buffer (150 mM NaCl, 1% Triton X-100, 0.1% SDS) and a high salt buffer (500 mM NaCl, 1% Triton X-100, 0.1% SDS), followed by a lithium salt buffer (0.25 M LiCl, 1% NP40, 1% deoxycholic acid). Chromatin was eluted with 1% SDS and 0.1 M NaHCO₃ solution, and the cross-link was reversed at 65°C overnight. The DNA was treated with RNase for 20 min, proteinase K for 1 hour at 50°C, prior to phenol-chloroform purification, and ethanol precipitation. DNA samples were dissolved in TE buffer, blotted onto a N+ Hybond membrane (GE Healthcare) using a slot blot apparatus, and hybridized with the same probe as used for the trioxsalen experiments. Membranes analysis was performed as described for trioxsalen experiments. For TRF2, RAP1 and TIN2 ChIP the following antibodies were used: Rabbit polyclonal anti-RAP1 from Bethyl (A300-306A); Rabbit polyclonal anti-TIN2 from Abcam (ab64386); Rabbit polyclonal anti-TRF2 from Novus Biologicals (NB110-57130).

TERRA slot blot

RNA was extracted from 5 million HeLa cells treated (or not) with doxycycline as described above and transduced by the Empty, TRF2, or Top-less expressing vectors (see below for transduction conditions) using the RNAeasy kit from Qiagen. RNA (20 µg) from each condition was digested with 2 units of RNase free DNaseI (New england Biolabs) at 37°C for 10 min and heated at 75°C for 10 min. From these, 10 µg were digested with 1 µg of RNase (Life Technologies) at 37°C for 10 min. A total of 5 µl of 5× loading buffer (80 mM MOPS, 6 mM

EDTA, 2.6% formaldehyde, 30% formamide, 20 mM sodium acetate) was added and the samples were heated at 75°C for 10 min before slot blotting using a N+ Hybond membrane (GE Healthcare). Before and after slot blotting, wells were washed with 200 µl of 10x SSC. After UV crosslinking of the membrane and baking at 80°C during 15 min, bands were revealed by sequential hybridization in Church buffer with a telomeric probe (the same used for Trioxsalen experiments) and a probe obtained from a 500-bp fragment corresponding to the sequence of the human 26S RNA (precursor of 18S RNA (Vincent et al., 1993)). Membranes analysis was performed as described for trioxsalen experiments.

Immunofluorescence detection of telomere dysfunction-induced foci

Slides were fixed with 4% formaldehyde in PBS at room temperature for 10 min, and then incubated for 90 min with blocking buffer (PBS, 1% Triton X-100, 1% BSA and 5% Donkey serum), followed by incubation overnight at 4°C with anti-TRF1 (sc-6165; Santa Cruz Biotechnology) and anti- γ H2AX (05-636; Upstate) antibodies. Cells were then washed with PBS and incubated with anti-rabbit Alexa488 (A21206; Molecular probes) and anti-mouse Alexa555 (A31570; Molecular probes) antibodies. After washing with PBS, the nucleus was labeled with DAPI (VECTASHIELD mounting medium with DAPI, Vector Laboratories). For IF-PNA FISH labelling, slides were first treated as above using a rabbit anti-53BP1 antibody (NB100-305; Novus Biological) followed by a goat anti-rabbit Alexa 488 antibody (111-545-144; Jackson ImmunoResearch) then fixed again with 4% formaldehyde in PBS at room temperature for 2 min, de-hydrated by successive incubation in 50%, 75% and 100% ethanol for three min. Hybridization was performed at 80°C in 70% Formamide, 10 mM Tris pH 7.2 for three min followed by an incubation overnight at room temperature. Slides were washed first in the Formamide, Tris solution above, then in a 150 mM NaCl, 50 mM Tris pH 7.5 solution and finally PBS. Mounting was performed as above.

IF images were produced using a Zeiss LSM 5 Exciter confocal laser scanning microscope (Zeiss, Jena, Germany) and analyzed using the ZEN software. PNAFISH/IF images were obtained on a DeltaVision Elite microscope (GE Healthcare).

Metaphase spreads analysis

For chromosome analysis, cells were arrested in metaphase for 3 hours at 37°C with 50 ng/ml of colcemid (KaryoMAX, Invitrogen). Cells were incubated for 15 min at 37°C in hypotonic solution (75 mM KCl), fixed in methanol:acetic acid (3:1), and spread on cold, wet, ethanol-cleaned slides. Slides were fixed in 4% formaldehyde in PBS for 2 min, washed in PBS, digested with pepsin (0.5 mg/ml, 0.01 N HCl) for 10 min at 37°C, washed in PBS, fixed in 4% formaldehyde in PBS for 2 min, washed in PBS, dehydrated in increasing concentrations of ethanol, and air-dried. Hybridization was then performed using FITC-conjugated (CCCTAA)₃ PNA probe (Panagene) diluted at 50 nM in 70% formamide, 10 mM Tris-HCl (pH 7.2), and 1% blocking reagent (Roche). Slides were denatured at 80°C for 3 min at room temperature, and hybridization was performed at room temperature in a moist chamber in the dark for 2 hours. Slides were washed twice for 15 min in 70% formamide and 10 mM Tris-HCl (pH 7.2) and three times for 5 min in 50 mM Tris-HCl pH 7.5, 150 mM NaCl, and 0.05% Tween-20 at room temperature. Slides were washed in PBS and mounted in VECTASHIELD with DAPI (Vector laboratories).

Metaphase spreads were visualized on an epifluorescence Axioimager Z2 microscope and analyzed using the metasytem ISIS software.

2D gels

DNA (5 µg) extracted from HeLa cells treated with or without doxycycline as described above and transduced with Empty, TRF2, or Top-less expressing vectors was migrated on an 0.5% agarose in 1× TBE (15-cm gel at 130 V) until the xylene dye was 2 cm from the bottom of

the gel. Bands were cut and placed horizontally for a second-dimension electrophoresis performed in 0.5 µg/ml ethidium bromide and 1× TBE (both in the gel and the running buffer). Markers were run beside each sample band. Migration was performed at 50 V for 14 hours. After migration, DNA was transferred onto a membrane, telomeric DNA was revealed and data were analyzed as above (Trioxsalen experiments).

Overhang assay

The overhang assay was adapted from van Steensel *et al.*, 1998 (van Steensel et al., 1998). Briefly, 10 µg of genomic DNA from HT1080 cells expressing sh*TERF2* and transduced with either the Empty vector or vectors expressing the TRF2 or Top-less proteins (see above) were digested with 125 and 175 units of *Hinf*I and *Rsa*I (Promega), respectively, overnight at 37°C. After ethanol precipitation, the samples were divided in two; half was digested with 100 units of *E. coli* Exonuclease I (New England Biolabs) for 5 hours at 37°C. All samples were hybridized with 0.2 pmoles of a ³²P end-labeled single-stranded (CCCTAA)₃ probe overnight at 50°C. Hybridized samples were loaded on a 10-cm-long, 0.9% 1× TBE agarose gel and migrated at 6 V/cm for 75 min at room temperature. The gel was then dried on 3 MM paper for 4 hours at 40°C and exposed on a phosphorimager screen. Analysis was performed as described above on a Typhoon 9500. For denaturing conditions, an in-gel denaturing hybridization was performed on the dried gel, as described previously (Karlseder et al., 2002).

References

- Amiard, S., Doudeau, M., Pinte, S., Poulet, A., Lenain, C., Faivre-Moskalenko, C., Angelov, D., Hug, N., Vindigni, A., Bouvet, P., *et al.* (2007). A topological mechanism for TRF2-enhanced strand invasion. *Nat Struct Mol Biol* 14, 147-154.
- Bustamante, C., Keller, D., and Yang, G. (1993). Scanning force microscopy of nucleic acids and nucleoprotein assemblies. *Current opinion in structural biology* 3, 363-372.

Chen, D., Bowater, R., Dorman, C.J., and Lilley, D.M. (1992). Activity of a plasmid-borne leu-500 promoter depends on the transcription and translation of an adjacent gene. *Proceedings of the National Academy of Sciences of the United States of America* 89, 8784-8788.

Doksani, Y., Wu, J.Y., de Lange, T., and Zhuang, X. (2013). Super-resolution fluorescence imaging of telomeres reveals TRF2-dependent T-loop formation. *Cell* 155, 345-356.

Karlseder, J., Smogorzewska, A., and de Lange, T. (2002). Senescence induced by altered telomere state, not telomere loss. *Science* 295, 2446-2449.

Nettikadan, S., Tokumasu, F., and Takeyasu, K. (1996). Quantitative analysis of the transcription factor AP2 binding to DNA by atomic force microscopy. *Biochem Biophys Res Commun* 226, 645-649.

Pipkin, M.E., and Lichtenheld, M.G. (2006). A reliable method to display authentic DNase I hypersensitive sites at long-ranges in single-copy genes from large genomes. *Nucleic acids research* 34, e34.

Poulet, A., Buisson, R., Faivre-Moskalenko, C., Koelblen, M., Amiard, S., Montel, F., Cuesta-Lopez, S., Bornet, O., Guerlesquin, F., Godet, T., *et al.* (2009). TRF2 promotes, remodels and protects telomeric Holliday junctions. *EMBO J* 28, 641-651.

Poulet, A., Pisano, S., Faivre-Moskalenko, C., Pei, B., Tauran, Y., Haftek-Terreau, Z., Brunet, F., Le Bihan, Y.V., Ledu, M.H., Montel, F., *et al.* (2012). The N-terminal domains of TRF1 and TRF2 regulate their ability to condense telomeric DNA. *Nucleic acids research* 40, 2566-2576.

Rivetti, C., and Codeluppi, S. (2001). Accurate length determination of DNA molecules visualized by atomic force microscopy: evidence for a partial B- to A-form transition on mica. *Ultramicroscopy* 87, 55-66.

Simonet, T., Zaragosi, L.E., Philippe, C., Lebrigand, K., Schoutedden, C., Augereau, A., Bauwens, S., Ye, J., Santagostino, M., Giulotto, E., *et al.* (2011). The human TTAGGG repeat factors 1 and 2 bind to a subset of interstitial telomeric sequences and satellite repeats. *Cell Res* 21, 1028-1038.

van Steensel, B., Smogorzewska, A., and de Lange, T. (1998). TRF2 protects human telomeres from end-to-end fusions. *Cell* 92, 401-413.

Vincent, S., Marty, L., and Fort, P. (1993). S26 ribosomal protein RNA: an invariant control for gene regulation experiments in eucaryotic cells and tissues. *Nucleic acids research* 21, 1498.